Summer 2022

Analytical Modeling of a Novel Elastohydrodynamic Seal Design for Supercritical CO2 Power Cycles

Ikenna C. Ejiogu

ANALYTICAL MODELING OF A NOVEL ELASTOHYDRODYNAMIC SEAL DESIGN FOR SUPERCRITICAL CO_2 POWER CYCLES

by

IKENNA CYRIL EJIOGU

(Under the Direction of Sevki Cesmeci)

ABSTRACT

Supercritical carbon dioxide (sCO_2) power cycles show great potential for higher plant efficiencies and power densities for a wide range of power generation applications such as fossil fuel power plants, nuclear power production, solar power, and geothermal power generation. sCO_2 leakage has been one of the main concerns in such applications, penalizing the cycle efficiencies. The effect of the seal leakage on the cycle efficiency could be as high as 0.65% for a utility sCO_2 power cycle. Therefore, there is a pressing need for effective sealing solutions to get the full benefit of sCO_2 power generation technology. To offer a potential solution, we propose an Elasto-Hydrodynamic (EHD) seal that can work at elevated pressures and temperatures with low leakage and minimal wear. The EHD seal has a very simple, sleeve like structure, wrapping on the rotor with minimal initial clearance at 25 to 50μm levels. In this work, a proof-of-concept study for the proposed EHD seal was presented by using the Reynolds equation, Lame's formula, Barus Equation, and Dowson-Higginson formula to model the pressure distribution along the seal clearance as well as the seal deformation. The analytical modeling of the seal was carried out in MATLAB using its built-in ordinary differential equation solver. The seal was evaluated for a 2" diameter test seal with a pressure range of 0.2MPa to 20MPa. At the high pressure of 20MPa, the clearance height at the throat (h_t) was found to be 24.7μm which is about 50.6% than the initial seal clearance (h_0) of 50μm, which resulted in a mass flow rate of 0.00162 kg/s. Also, a parametric

study was conducted to see the effects of the seal thickness, shaft diameter, and seal length on the performance of the seal. The results showed that all three geometric parameters play a major role in the seal deformation and the mass flow rate of the seal. For the seal thickness, the mass flow rate increased as the seal thickness increased. It resulted to be 0.00161 kg/s and 0.004055kg/s for seal thickness 0.5mm and 2.0mm, respectively at 20MPa. An increase in the shaft diameter led to a decrease in mass flow rate with 0.00187 kg/s and 0.00125 kg/s for 25mm and 50mm respectively at 20MPa. For the seal length, the mass flow rate decreased with increasing seal length with 0.00255 kg/s and 0.001185 kg/s for seal lengths of 13mm and 28mm respectively at 20MPa. The presented analytical study lays a solid foundation for future model developments that could be used in the design of the proposed EHD seal.

INDEX WORDS: Supercritical carbon dioxide, sCO_2, Seal, Elastohydrodynamic, Turbomachinery, MATLAB, Ordinary differential equation.

ANALYTICAL MODELING OF A NOVEL ELASTOHYDRODYNAMIC SEAL DESIGN FOR SUPERCRITICAL CO_2 POWER CYCLES

by

IKENNA CYRIL EJIOGU

B.S., Georgia Southern University, 2019

A Thesis Submitted to the Graduate Faculty of Georgia Southern University in Partial

Fulfillment of the Requirements for the Degree

MASTER OF SCIENCE

ANALYTICAL MODELING OF A NOVEL ELASTOHYDRODYNAMIC SEAL DESIGN FOR SUPERCRITICAL CO_2 POWER CYCLES

by

IKENNA CYRIL EJIOGU

Major Professor:	Sevki Cesmeci
Committee:	Priya Goeser
	Prakashbhai Bhoi

Electronic Version Approved:

July 2022

DEDICATION

I am pleased to dedicate this achievement to my dad, Uche Ejiogu for his tireless support to always be there for me not just financially to see that I graduate with both my bachelor's and master's degree but also his constant advice and guide to stay focused and achieve excellence. And to my mom, Oby Ejiogu who is always there to listen to me whenever I felt down and made me feel better to keep going. This won't have been possible without them both.

ACKNOWLEDGMENTS

First and foremost, I would like to thank God for giving me His grace to complete this thesis. I would like to acknowledge and thank my research advisor, Dr Sevki Cesmeci for his constant patience and support in coaching and guiding me during this process. He has helped me grow not only as a researcher but also as an engineer. My special thanks to my other committee members Dr. Goeser and Dr. Bhoi for supporting and being there for me. Also, I want to say a big thank you to Dr. Rony Rahman for his time in helping and training me.

I would also like to acknowledge the DOE for helping sponsor this project and making it a reality.

TABLE OF CONTENTS

LIST OF TABLES

Page

LIST OF FIGURES

Page

ABBREVIATIONS

EHD: Elasto-Hydrodynamic

sCO_2: Supercritical CO_2

ODE: Ordinary Differential Equation

d_{shaft}: Diameter of the shaft

t_{seal}: Thickness of the seal

L_{seal}: Length of seal

E: Young's modulus

D: Internal diameter

D_0: External diameter

h_0: Initial seal clearance

h_t: Throat height

h_x: Throat location

CHAPTER 1

INTRODUCTION

1.1 Purpose of Study

For many years following the industrial revolution, global industries have depended on fossil fuels and steam for power generation which is transformed into electricity using thermodynamic power cycles. Sadly, this dependence on fossil fuels production for electricity supply has had a negative impact on the atmosphere, resulting in greenhouse pollution which also contributes to global warming. Current thermodynamic power cycles like the Rankine and Brayton typically use water and air respectively as the working fluid to operate. However, with the urge of increased thermal efficiencies and tackling some of the challenges faced with the existing power cycles, the use of other working fluids is being considered. This has led to the emergence of supercritical CO_2 power cycles to help combat the negative impact. These power cycles require high operating conditions at the supercritical level like high temperatures and pressures of 350-700 $^{\circ}$C and 20-30 MPa on a 10-600 MWe scale. Supercritical CO_2 (sCO_2) holds great potential in nuclear power industries because CO_2 is an inexpensive working fluid and when paired with the high operating conditions used in these industries, the combination produces high thermal efficiencies compared to other power cycles like the Rankine, Brayton, or steam power cycles. However, despite these advantages, one of the challenges still at the developmental stages of research is the lack of suitable shaft seals to accommodate for the supercritical conditions. Over time with continuous use, the seals start to wear out. Hence, the leakage rate also increases. This study proposes a novel Elasto-Hydrodynamic (EHD) that can withstand the high temperature and pressure conditions, offering low leakage rate, minimal wear, and no stress concentration. The

purpose of this study was to develop an analytical modeling with sound scientific approach, which could later be tailored for more accurate models for the design of proposed seal concept.

1.2 Uniqueness of This Study

In this study, we adopted a proven analytical modeling approach that has been applied for different flow geometries and configurations. Namely, we employed the famous Reynolds equation, which has been widely used in the EHD lubrication theory to model the flows in narrow channels in angular direction such as in the case of journal bearings. However, in this study, we applied the Reynolds equation model to analyze fluid flow in a narrow channel in the axial direction along with thick-walled cylinder equations for the deformation of the seal. The proposed approach has not been applied for the proposed seal design previously

1.3 Research Hypothesis

A new design of EHD seal is proposed and analyzed numerically to see the effect of the operating pressure on seal deformation and mass flow rate. This proposed seal is novel of its kind and expected to produce low leakage, low wear, and tear at a minimal cost with no stress concentration when subjected to high operating conditions such as high pressure and temperature. If an analytical model can be used to describe seal behavior, then the proposed seal concept can be proven theoretically.

CHAPTER 2

LITERATURE REVIEW

The idea of sCO_2 power cycles was first proposed by Sulzer in 1950 (White et al. 2021). The use of CO_2 power cycles has been proposed as a viable option for the need to fulfill a more reliable, clean energy to power systems. The idea to go from fossil fuel/hydro energy to clean energy like CO_2 has been vastly implemented in many countries of the world. For example, in the article published by the Chinese government sent to the UN to set the objective of climate change, it is stated that the government's goal is to reach peak carbon dioxide emissions around 2030 and decrease by 60-65% per unit of GDP from 2005 levels with non-fossil energy consumption accounting for 15% of the total energy consumption (White et al. 2021). Other countries have followed suit and are putting great attention in terms of research and growth of sCO_2 power cycles. The potential in the growth of sCO_2 is being validated by all the research, and the financial help various countries of the world are putting forth towards its technological developments (Cesmeci et al. 2021). Some of the first research for sCO_2 was done by (Feher 1968) where a simple thermodynamic supercritical power cycle was studied, and the responsiveness of the cycle was assessed and compared with the operating conditions. The critical temperature and pressure point for CO_2 is 31°C (304K) and 73.8 bar (7.38 MPa) respectively (See Figure 1). It reaches supercritical state when it goes above the critical point for the temperature and pressure causing there to be no distinction between the liquid and gas phases (Patel 2019) while adopting a unique characteristic as it can behave like a single-phase fluid.

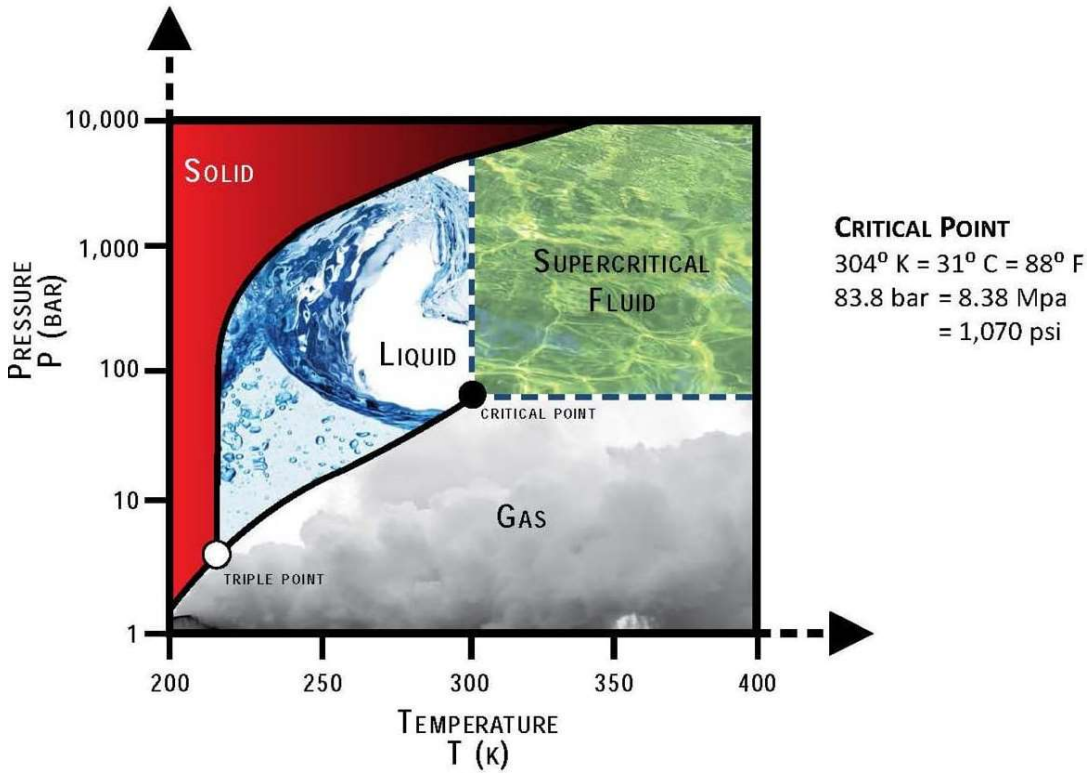

Figure 1: Critical point of sCO2 (Patel 2019)

CO_2 is the ideal fluid for a closed loop Brayton cycle in nuclear power generation systems which is a low-cost fluid that is nontoxic, non-flammable, non-corrosive and readily available (Persichilli et al. 2012). CO_2 when used as the working fluid can operate at high temperature and pressure ranging from 350°C to 800°C thereby producing higher thermal efficiencies (White et al. 2021). Figure 2 shows how the thermal efficiencies vary for sCO_2, helium, nitrogen, Brayton cycles superheated and supercritical Rankine cycles with the inlet temperature being the dependent factor (Ahn and Lee 2014). These supercritical CO_2 power cycles are becoming more popular and sought out by nuclear power industries because of their efficiency and compatibility advantage compared to other power cycles like the steam, closed Rankine, open Brayton, or air based. Its efficiency can be attributed to its ability to adopt properties midway as both a gas and a liquid (supercritical state) which makes it effectively used throughout the entire closed Brayton cycle

enabling them to have enormous potential in fossil fuel power industries, nuclear power industries, geothermal power industries and waste heat recovery systems.

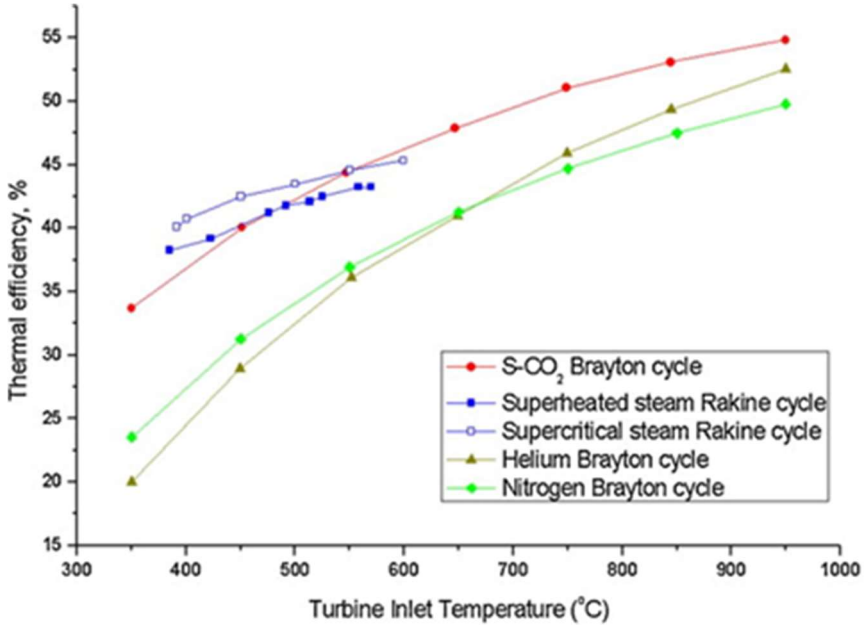

Figure 2: Thermal efficiencies of various power cycle systems varying with turbine inlet temperature (Ahn and Lee 2014).

However, for the machine components, heat exchangers and other parts used in the sCO_2 power cycle systems to be able to withstand these high operating temperatures and pressures at supercritical conditions, there are still technological hurdles to address in the design as well as material selection and sensitivity to CO_2 of these components. One of them notably is the lack of appropriate shaft seals for the operating conditions of sCO_2 power cycles. Achieving tighter clearances between the stationary and rotary component remains one of the main challenges encountered in the design stage for these turbomachinery components. This solely is one of the main causes of leakage in the turbomachinery systems. Since most sCO_2 power cycles are designed for the fluid conditions at the inlet of the compressor to be close to the critical point and because the fluid properties of CO_2 near the critical point is changing rapidly, it is also difficult to predict

the seal leakage using the current methods of technology (Bennett et al. 2018). Development of the machine components for large scale sCO_2 power cycles are still in its early stages. It was found in a recent study that by using the current sealing technology on a 450MWe utility scale, thermodynamic cycle efficiencies would be penalized by 0.65 percent points on a 51.9% efficient power cycle, and it costs roughly about $12 per kW for 1%-point efficiency which ends up totaling to about $3.5M loss for each cycle (Bidkar et al. 2017). Furthermore, the excessive sCO_2 losses and leaks would result in more additional costs because they would have to be recompressed back in vapor form into the system since they operate on closed loop cycles which is not the case for other power cycles like the steam power cycle where steam can be turned back into water and used again. This is the reason why low leakage CO_2 seals are very important in the design and implementation stage for these sCO_2 power cycles to maximize their full potential while maintaining their competitiveness in the nuclear power industries for generations to come.

In this thesis, the analytical modeling of a new elasto-hydrodynamic seal concept would be proposed, which can be used in these sCO_2 power cycles. But first, we need to understand some of the existing sealing methods used in our present power generation industries. Sealing can come in two forms: Dynamic sealing and Static sealing. In dynamic sealing, there is some form of motion that exists at the boundary between the mating surfaces either with a stationary and rotating component or two relatively rotating components. It could be a reciprocating, oscillating or rotary motion. On the other hand, static sealing involves when there is no relative motion between the mating surfaces. It can either be a radial or axial static seal. Some common examples of static seals are O rings, V rings, gaskets, nozzles, and bonded seals. Materials used in the making of dynamic seals need to be carefully selected because they are prone to wear and tear faster due to the constantly moving parts/faces. This means the parts need to be made naturally stronger and

lubricated more often than static seals to be able to utilize and improve its shelf life to the maximum. The focus here would be more on the dynamic sealing technology as its mechanism corresponds to the seal design we want to innovate. Some examples of dynamic seals include labyrinth seals, rubber lip seals, rotary mechanicals seals, brush seals. Next, we look at some of the characteristics of these seal types and see how they compare to others in the sealing industry.

2.1 Labyrinth seals

Labyrinth seals are the most used seals in the turbomachinery industry because of their ability to operate at high rotational speeds. They are clearance seals which are usually mounted on the rotor and come in various configurations (see Figure 3) like straight, interlocking, slanted, stepped or a combination of both (Chupp et al. 2007). They require an operating clearance to prevent contact from the rotary and stationary components. Although labyrinth seals are effective in confining the flow, they do not react well to the dynamic effects caused by the rotary components and frequently lead to turbomachinery issues. This issue was addressed by (Muszynska 2001) and (Childs and Ramsey 1991) in their paper with the introduction of a swirl brake at the seal inlet to help reduce the surrounding velocities of the rotary components. They found positive correlation with the swirl brake in destabilizing the dynamic forces when compared without a swirl brake.

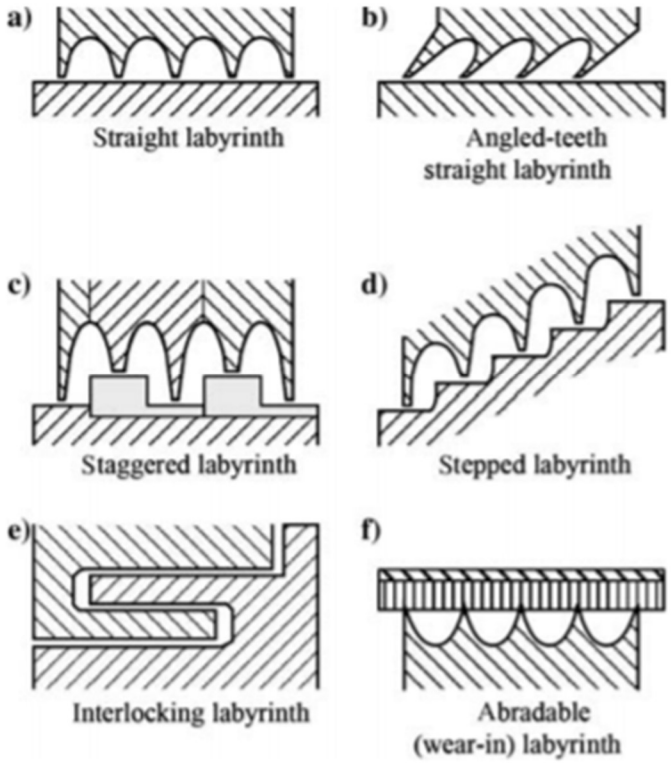

Figure 3: Labyrinth seal configurations (Chupp et al. 2007).

Since they are designed with large radial clearances to avoid contact with the rotor, that may cause overheating and damage to it thereby increasing leakage rate which also has a positive correlation with the performance (Aksit et al. 2004). Despite this, they are still widely used in the turbomachinery industry because of their proven reliability and robust operation.

2.2 Brush seals

On the other hand, brush seals were designed to be a better alternative compared to labyrinth seals. The first endeavor to replace labyrinth seals with brush seals was first done in 1955 by General Electric J-47 engine but were unsuccessful at the time until Rolls Royce incorporated them in demonstrator engines in 1980 (Cieślewicz 2004). A typical brush seal usually consists of a front plate, back plate and a bristle pack. The brush is usually mounted on the stationary part of the engine and has a direct contact with the rotating elements which helps to reduce unwanted

leakages in the flow (Kudriavtsev and Braun 1996). This gives it a comparative advantage compared to labyrinth seals. Some other advantages compared to labyrinth seals include: a more reduced weight, smaller axial space requirements and accommodation of shaft excursions (Chupp et al. 2007). However, the wear and tear caused by the bristle contact with the rotor continues to remain an issue in brush seals and the dynamic instabilities introduced when multiple seal arrangements are used. Atkinson and Bristol (1992) studied the effect of wear and tear caused in the bristle and rotor by using bristle materials made of cobalt and nickel-based alloys and coating materials made of chromium, carbide, tungsten carbide and aluminum oxide. They concluded that the wear and tear is temperature dependent of the material.

2.3 Film-riding seals

The film-riding seal is another sealing type used in turbomachinery. They are a non-contact seal which means they don't touch the rotating shaft and are becoming more popular in sCO_2 applications due to these which yields to minimal heat generation and power loss (Zheng and Berard 2008). They are designed to have faces that separate through the application of differential pressure, relative motion of the faces or a combination of both (Munson 1993). Tibos, Teixeira, and Georgakis (2017) investigated in their paper the most effective groove type to be used in film riding seals between the inclined groove, Rayleigh step and herringbone groove and found that the Rayleigh step offers the strongest level of combined hydrostatic and hydrodynamic load support while also being easier to mesh on individual seal segments. However, at low pressure conditions (close to vacuum) these groove designs may not be able to generate the needed film stiffness because of the low air density which restricts the hydrodynamic effectiveness (Zheng and Berard 2001). This remains one of the challenges faced when using groove designs in film riding seals.

2.4 Hybrid Floating Brush Seal

Lattime (2000) in their paper came up with an innovative design called the Hybrid Floating Brush Seal (HFBS) (See Figure 4) to help reduce the wear and tear associated with the current brush and labyrinth sealing technologies by combining a rotating brush seal and film riding face seal that allows both axial and radial excursions at the sealed shaft to produce a non-contacting seal. The brush seal which acts like the primary seal rotates along the shaft which floating against a hydrodynamic film riding face seal which act as the secondary seal. This phenomenon helps reduce the wear and tear caused by the bristles of the brush seal because the speed of contact surface region between the bristles and rotor is removed. HFBS seal design uses a higher radial interference between the rotor and bristle which allows the brush to track the shaft as it rotates and form a tighter seal around the circumference ultimately reducing seal leakage and improving its performance.

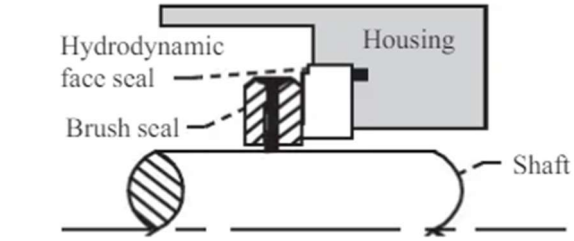

se

Figure 4: Hybrid Floating Brush Seal (HFBS) (Lattime 2000).

2.5 Mechanical Face seals

A mechanical face seal is another form of a contact seal where the contact is usually on the face of a housing or shaft. They can be seen used in heavy duty trucks were durability and ability to resist wear and tear is key because of the harsh environments these trucks are expected to withstand. Some examples of mechanical face seals include gaskets, spring seals and O rings. A mechanical face seal design essentially consists of a primary ring, mating ring, spring, secondary seal, housing. The sealing rings in contact with each other during use are the primary and mating

ring. The mating ring is the stationary part and is mounted firmly on either the shaft or the housing. The mating ring can also be called the guided ring. The primary ring is mounted flexibly on the shaft to allow for some axial or angular motion when the system is in use. The secondary seal provides some additional sealing protection to the primary ring and mating ring to make sure they are self-aligned and close to each other during use. The spring is designed to keep the mating and primary rings pushed together and helps to adjust the compression when the two rings in contact begin to wear slowly over time.

Some of the operating properties like temperature and pressure of the various seal types are shown in the Table 1 below (Cieślewicz 2004). The current sealing technologies would not be able to withstand the desired temperature of 350-700˚C and desired pressure of 20-30 MPa on a 10-600 MWe scale.

Table 1: Operating conditions for some turbomachinery sealing technologies (Cieślewicz 2004).

Seal type	**Pressure (MPa)**	**Temperature (K)**	**Surf. Speed (m/s)**	**Material**
Face	1.034	811	145	Carbon
Labyrinth	1.724-2.758	978	457	Ni Superalloy Teeth + Abradable
Brush	0.551-0.689/ stage	978	305	Cobalt Superalloy

2.6 Journal Bearings

Next, Journal bearings are explained to show a similar concept used for this mechanism and one of applications of the Reynolds equation for a rotary machine. Journal bearings could be of two forms: hydrodynamic and elasto hydrodynamic. The term ‘hydrodynamic’ used in journal bearing defines it in which the bearing face is separated from the journal face by the film generated from the lubrication when it is rotating. The latter takes account of the elastic deformation due to

the pressure and other related variables. The elasto hydrodynamic journal bearing can be returned to its original shape if expanded. Elasto-hydrodynamic lubrication occurs when the film pressure increases until it alters/deforms the shape of the film thickness (See Figure 5). The Reynolds equation is the governing equation used to explain the pressure and fluid flow through a journal bearing. It would be further explained and expanded upon in Section 2.7 and 2.7.1. The Reynolds equation is not the same as the Reynolds number, this is a common misconception made. Although they were founded by the same person Osborne Reynolds in the middle 1800s, the Reynolds equation includes a partial differential equation modified from the longer Naiver-Stokes equation to a shorter and simplified version. With the addition of this PDE, it means that the Reynolds equation cannot be used analytically to solve lubrication problems and requires a numerical method such as a finite element technique to solve it. This gave rise to the birth of the Reynolds number which can be used to solve the lubrication problems analytically. The Reynolds equation also does not take account of the inertia and viscous effects of the fluid whereas the Reynolds number does.

2.6.1 Lubrication in Journal Bearings

Lubrication is an essential process in the operation of machine parts as it can help reduce wear, friction of a material and reduction of excessive power. It can be a hydrodynamic lubrication or a boundary lubrication. Boundary lubrication focuses on the lubrication when metal to metal is involved with two sliding surfaces while hydrodynamic lubrication occurs when a working clearance is created by the fluid film between the journal bearing and rotary shaft (lubricant domain). The focus here would be on the hydrodynamic lubrication. This process helps rotary machines to slid past each other easily when solid to solid contact is involved by creating a clearance. It can be in the form of oil and water. Oil lubricated bearings have more viscosity than

water lubricated bearings which means that they are stiffer when pressure is continually applied on it. On the other hand, water lubricated ones are more friendly with the environment as they produce no little to no residue and no pollution is released in the environment.

2.6.2 Mechanism of Journal Bearings

Since the two cylinders representing the bearing domain and the lubricant domain are eccentric to each other and have the same center, when the shaft is at rest the highest pressure would be vertically downwards on the edge of the bearing and the lubricant would be uniformly distributed between the left and right sides of the bearing. As the shaft is powered on and begins to rotate gradually, the pressure is highest as the lubricant fills the contact zone between the two cylinders whether in a clockwise motion or an anti-clockwise motion. As the speed continues to rapidly increase, the highest pressure continues to rapidly change as it rotates so the film continues to get used up and gets smaller and smaller. This is one disadvantage of hydrodynamic lubrication because the user or operator must constantly feed the machine the lubricant from time to time to ensure that the solid cylinders do not touch each other while rotating.

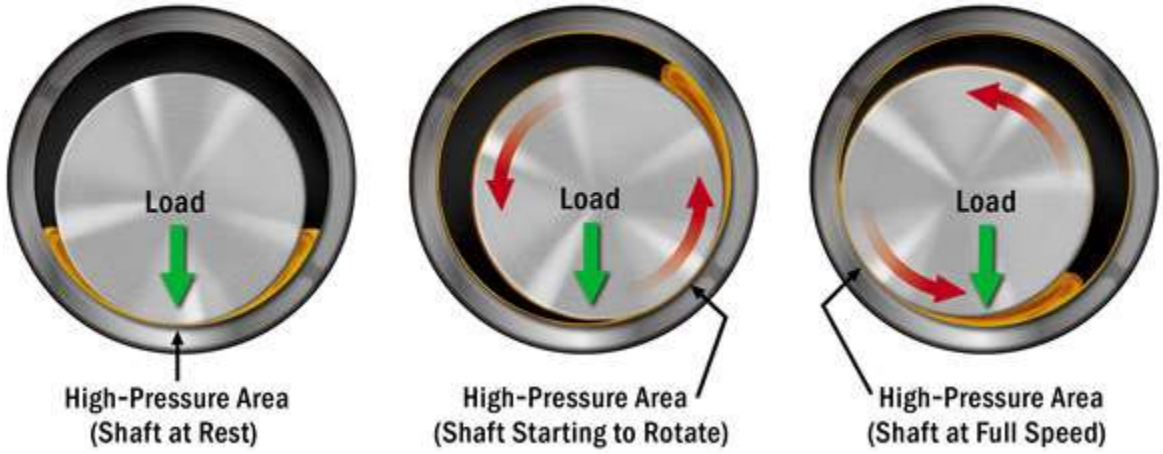

Figure 5: Mechanism of a Journal Bearing

2.6.3 Addition of Slip Analysis

The main difference between the hydrodynamic and elastohydrodynamic lubrication is the presence of the elastic deformation in the latter and Attia Hili et al. (2010) conducted a study to see the effect of this elastic deformation on the two models. It helped study this and found that the influence of elastic deformation increases the pressure and the minimum film thickness in the bearing which shows that the flexibility of the bearing linear indeed plays an important role in the operation of a journal bearing (Attia Hili et al. 2010). The slip and no slip boundary conditions are another important note when considering the behavior of fluid and solid interaction. Although the no slip condition is frequently used when contact surfaces are involved it is not always the best option available as some surfaces can show some slip at the boundary which led to another design done with the introduction of a slip/no slip boundary condition on the journal bearing. Fortier and Salant (2005) investigated this effect by the addition of slip to the bearing surface region to see how it affects the friction force, leakage rate and film thickness. They found that with the addition of a slip on the journal surface, it improves all the parameters tested and leads to better bearing performance. Hunter and Zienkiewicz (1960) focused their research on looking at the effect of the temperature variations on the lubricant films from hydrodynamic lubrication. They saw that it was by no means to neglect the effect of viscosity and the temperature variations as they produced lower resultant pressures. To improve this, it would be better to allow for a viscosity change in the bearing direction.

2.7 Concept of the Reynolds equation

The concept of hydrodynamic lubrication was experimentally studied by Osborne Reynolds who helped reduce the Navier-Stokes equations into a more understandable second order differential equation for the pressure within the bearing surfaces. Assumptions must be made

before the Reynolds equation can be valid and implemented in any fluid flow problem. They include laminar (low Reynolds number) flow in the lubricant, Newtonian fluid like water or honey (no slip at the boundaries), inertia and body forces are small or negligible, the fluid must be incompressible, the pressure is constant in the direction perpendicular to the flow (dp/dy=0) and it should be an isothermal process. Myant et al. (2010) investigated a method of obtaining the film thickness when a material can easily be deformed under low pressure using optical interferometry method. It is not a very easy process to attain as the film thickness can have a wide range of values which is not easy to predict. They found that the outlet of the bearing is much more responsible for the load carrying capacity. With detailed explanation, Mertz (2019) helped simplify the Reynolds equation from the Navier-Stokes equation to a dimensionless parameter that can be used when dealing with no units. This equation assumes that the pressure does not vary in the film thickness direction and the inertia is ignored. Peiran and Shizhu (1990) looked at another way of constructing the Reynolds number to take account for density and viscosity variations in the film thickness because of temperature and shear thinning effects. The impact of the non-Newtonian conduct of the lubricant isn't as significant as that of the thermal one (Peiran and Shizhu 1990). A model was simulated, and the Reynolds equation was modified to take account of the inertia and recirculation effects which is usually ignored from the original modified Reynolds equation when dealing with hydrodynamic lubrication surfaces, but they ignored the cavitation (Rom and Müller 2019). They compared their results with the original Reynolds equation and found their equation to be accurate also where the results for the load carrying capacity deviated only about 2% and speed ups of about 676 were achieved when compared to the original equation (Rom and Müller 2019). The derivation of the famous Reynolds equation from the Navier-Stokes equation would be studied in the next section.

2.7.1 Derivation of the Reynolds equation

The derivation of the Reynolds equation begins first by defining the equations of motion from the Naiver-Stokes equation in cartesian co-ordinates shown below:

$$\rho\frac{Dv_x}{Dt} = \rho X - \frac{\partial p}{\partial x} + \frac{2}{3}\frac{\partial}{\partial x}\mu\left(\frac{\partial v_x}{\partial x} - \frac{\partial v_y}{\partial y}\right) + \frac{2}{3}\frac{\partial}{\partial x}\mu\left(\frac{\partial v_x}{\partial x} - \frac{\partial v_z}{\partial z}\right) + \frac{\partial}{\partial y}\mu\left(\frac{\partial v_y}{\partial x} + \frac{\partial v_x}{\partial y}\right) + \frac{\partial}{\partial z}\mu\left(\frac{\partial v_x}{\partial z} + \frac{\partial v_z}{\partial x}\right) \quad (1)$$

$$\rho\frac{Dv_y}{Dt} = \rho Y - \frac{\partial p}{\partial y} + \frac{2}{3}\frac{\partial}{\partial y}\mu\left(\frac{\partial v_y}{\partial y} - \frac{\partial v_x}{\partial x}\right) + \frac{2}{3}\frac{\partial}{\partial y}\mu\left(\frac{\partial v_y}{\partial y} - \frac{\partial v_z}{\partial z}\right) + \frac{\partial}{\partial x}\mu\left(\frac{\partial v_x}{\partial y} + \frac{\partial v_y}{\partial x}\right) + \frac{\partial}{\partial z}\mu\left(\frac{\partial v_y}{\partial z} + \frac{\partial v_z}{\partial y}\right) \quad (2)$$

$$\rho\frac{Dv_z}{Dt} = \rho Z - \frac{\partial p}{\partial z} + \frac{2}{3}\frac{\partial}{\partial z}\mu\left(\frac{\partial v_z}{\partial z} - \frac{\partial v_x}{\partial x}\right) + \frac{2}{3}\frac{\partial}{\partial z}\mu\left(\frac{\partial v_z}{\partial z} - \frac{\partial v_y}{\partial y}\right) + \frac{\partial}{\partial y}\mu\left(\frac{\partial v_z}{\partial y} + \frac{\partial v_y}{\partial z}\right) + \frac{\partial}{\partial x}\mu\left(\frac{\partial v_z}{\partial x} + \frac{\partial v_x}{\partial z}\right) \quad (3)$$

v_x, v_y and v_z represent the velocity profiles in the x, y and z directions. The parameters on the left-hand side account for the inertia forces while the parameters on the right-hand side account for the body force, pressure and viscosity respectively.

Next, the equation for mass conservation is stated as follows:

$$\frac{\partial\rho}{\partial t} + \frac{\partial\rho v_x}{\partial x} + \frac{\partial\rho_{\ y}}{\partial y} + \frac{\partial\rho_{\ z}}{\partial z} = 0 \quad (4)$$

where $\frac{\partial\rho}{\partial t}$ represents the change of mass/density with respect to time and $\partial\rho v_x$, $\partial\rho v_y$ and $\partial\rho v_z$ represent the velocity profile with relation to the mass/density in the x, y and z directions. This equation simply means that the mass of the system is constant with respect to time and the mass also remains constant for the velocities in the x, y and z directions. It is a closed system which

means that mass cannot be added or removed from the system but remains conserved over a time period.

In this case, the cartesian co-ordinates for the y and z profiles can be neglected because the fluid flows axially through the clearance in only the x direction. Since mass is conserved over time it can be assumed that the flow is incompressible, and the density can also be neglected. The inertia force on the left-hand side of the equation is also negligible because it's very small compared with the pressure and viscous parameters. With these assumptions taken account for, the equations of motion from above for the x component reduces to:

$$\frac{\partial p}{\partial x} = \frac{2}{3}\frac{\partial}{\partial x}\mu\left(\frac{\partial v_x}{\partial x} - \frac{\partial v_y}{\partial y}\right) + \frac{2}{3}\frac{\partial}{\partial x}\mu\left(\frac{\partial v_x}{\partial x} - \frac{\partial v_z}{\partial z}\right) + \frac{\partial}{\partial y}\mu\left(\frac{\partial v_y}{\partial x} + \frac{\partial v_x}{\partial y}\right) + \frac{\partial}{\partial z}\mu\left(\frac{\partial v_x}{\partial z} + \frac{\partial v_z}{\partial x}\right) \quad (5)$$

By integrating the conservation of mass equation with respect to z between 0 and h set as the limits we get:

$$\int_0^h \frac{\partial \rho}{\partial t} dz + \int_0^h \frac{\partial(\rho v_x)}{\partial x} dz + \int_0^h \frac{\partial(\rho v_y)}{\partial y} dz + [p v_z]_0^h = 0 \quad (6)$$

Now by evaluating the integrals containing ρv_x and ρv_y we arrive at:

$$\int_0^h \frac{\partial \rho}{\partial t} dz + h\left[\frac{\partial(\rho V_x)}{\partial x} + \frac{\partial(\rho V_y)}{\partial y}\right] - \frac{\partial}{\partial x}\int_0^h \left[\rho z \frac{\partial v_x}{\partial z} + z u \frac{\partial \rho}{\partial z}\right] dz - \frac{\partial}{\partial y}\int_0^h \left[\rho z \frac{\partial v_y}{\partial z} + z v \frac{\partial \rho}{\partial z}\right] dz +$$

$$[p v_z]_0^h = 0 \quad (7)$$

By combining the expressions for the velocity profiles v_x and v_y fully shown in Dowson (1962) with Equation 7, the combined equation becomes:

$$\frac{\partial}{\partial x}\left[(F_2+G_1)\frac{\partial p}{\partial x}\right]+\frac{\partial}{\partial y}\left[(F_2+G_1)\frac{\partial p}{\partial y}\right]=h\left[\frac{\partial(\rho V_x)}{\partial x}+\frac{\partial(\rho V_y)}{\partial y}\right]-\frac{\partial}{\partial x}\left[\frac{(Vx_2-V_{\ 1})(F_3+G_2)}{F_0}+Vx_1G_3\right]-$$

$$\frac{\partial}{\partial y}\left[\frac{(Vy_2-Vy_1)(F_3+G_2)}{F_0}+Vy_1G_3\right]+\int_0^h\frac{\partial\rho}{\partial t}dz+\rho[Vz_2-Vz_1] \quad \text{(8)}$$

and the terms F_0, F_1, F_2, F_3, G_1, G_2 and G_3 are substitutes for:

$$F_0=\int_0^h\frac{dz}{\mu} \quad (9)$$

$$F_1=\int_0^h\frac{zdz}{\mu} \quad (10)$$

$$F_2=\int_0^h\frac{pz}{\mu}(z-\bar{z})dz \quad (11)$$

$$F_3=\int_0^h\frac{\rho z}{\mu}dz \quad (12)$$

$$G_1=\int_0^h[z\frac{\partial\rho}{\partial z}(\int_0^z\frac{z}{\mu}dz-\bar{z}\int_0^z\frac{dz}{\mu})]\,z \quad (13)$$

$$G_2=\int_0^h[z\frac{\partial\rho}{\partial z}\int_0^z\frac{dz}{\mu}]\,dz \quad (14)$$

$$G_3=\int_0^h z\frac{\partial\rho}{\partial z}\,dz \quad (15)$$

Notice that all the G formulas (G_1, G_2, G_3) have some form of $d\rho(density)$ term contained in the equation. In this case, the fluid is incompressible which means that the density is constant and not changing across the fluid so all the G terms can be neglected or equal to 0. This reduces Equation 8 to become:

$$\frac{\partial}{\partial x}\left[F_2\frac{\partial p}{\partial x}\right]+\frac{\partial}{\partial y}\left[F_2\frac{\partial p}{\partial y}\right]=h\left[\frac{\partial(\rho V_x)}{\partial x}+\frac{\partial(\rho V_y)}{\partial y}\right]-\frac{\partial}{\partial x}\left[\frac{F_3}{F_0}(Vx_2-Vx_1)\right]-\frac{\partial}{\partial y}\left[\frac{F_3}{F_0}(Vy_2-Vy_1)\right]+$$

$$\int_0^h\frac{\partial\rho}{\partial t}dz+\rho[Vz_2-Vz_1] \quad \text{..... (16)}$$

Since the flow is only in the axial direction in this case, all terms containing ∂y can be neglected and equaled to zero which further reduces Equation 16 to:

$$\frac{\partial}{\partial x}\left[F_2\frac{\partial p}{\partial x}\right]=h\left[\frac{\partial(\rho Vx)}{\partial x}\right]-\frac{\partial}{\partial x}\left[\frac{F_3}{F_0}(Vx_2-Vx_1)\right]+\int_0^h\frac{\partial\rho}{\partial t}dz+\rho[Vz_2-Vz_1] \quad \text{..... (17)}$$

Also, by assuming we have a steady state process which means that time is constant thereby all terms with respect to ∂t can be equaled to zero. Equation 18 then becomes:

$$\frac{\partial}{\partial x}\left[F_2\frac{\partial p}{\partial x}\right]=h\left[\frac{\partial(\rho Vx_2)}{\partial x}\right]-\frac{\partial}{\partial x}\left[\frac{F_3}{F_0}(Vx_2-Vx_1)\right]+\rho[Vz_2-Vz_1] \quad \text{..... (18)}$$

To calculate the pressure distribution for fluid flow sealing problems, Vx_2=Vz_2=Vz_1=0 and the parameters of F_0, F_1, F_2 & F_3 become:

$$F_0=\frac{h}{\mu} \quad \text{..... (19)}$$

$$F_1=\frac{h^2}{2\mu} \quad \text{..... (20)}$$

$$F_2=\frac{\rho h^3}{12\mu} \quad \text{..... (21)}$$

$$F_3=\frac{\rho h^2}{2\mu} \quad \text{..... (22)}$$

Using the boundary conditions of Vx_2=Vz_2=Vz_1=0 listed above, Equation 23 is deducted to become:

$$\frac{\partial}{\partial x}\left[F_2\frac{\partial p}{\partial x}\right]=\frac{\partial}{\partial x}\left[\frac{F_3}{F_0}(Vx_1)\right] \quad \text{..... (23)}$$

Since the flow is in the axial direction, Vx_1 is the only velocity profile used for this case since flow is in the horizontal direction.

Substituting the terms of F_0, F_1, F_2, F_3, the simplified Reynolds equation becomes:

$$\frac{\partial}{\partial x}\left[\frac{\rho h^3}{12\mu}\frac{\partial p}{\partial x}\right]=\frac{\partial}{\partial x}\left[\frac{\rho h}{2}(Vx_1)\right] \quad \text{..... (24)}$$

The equation used to solve for velocity profile in the x direction (Vx_1) along the clearance region is shown as:

$$Vx_1=-\frac{1}{2\mu}\frac{dp}{dx}(h-y)y+U_0(1-\frac{y}{h}) \quad \text{..... (25)}$$

where p is the pressure, h is the film thickness, y is the term in the film thickness direction, U_0 is the initial speed and μ is the dynamic viscosity of the fluid.

The formula for calculating the mass flow/leakage rate Q, is given:

$$Q=\rho AVx_1 \quad \text{..... (26)}$$

where ρ is the density of the fluid, Vx_1 is velocity in the x direction and A is the area in the clearance region.

By substituting the terms for Vx_1 and integrating Equation 26 we get:

$$Q=\int_0^h \rho\pi D\left[-\frac{1}{2\mu}\frac{dp}{dx}(h-y)y+U_0\left(1-\frac{y}{h}\right)\right]dy \quad \text{..... (27)}$$

Evaluating the Equation 27 integral, we arrive at:

$$Q = \frac{\pi D}{12}\left(-\frac{\rho}{\mu}h^3\frac{dp}{dx} + 6U_0 h\right) \quad \text{..... (28)}$$

The initial speed U_0 is typically very small compared with the working pressure and its effect on the mass flow rate can be neglected. Therefore, the mass flow/leakage rate Q is simplified to:

$$Q = -\frac{\pi\rho D h^3}{12\mu}\frac{dp}{dx} \quad \text{..... (29)}$$

where ρ is the density of the working fluid, h is the film thickness, D is the Diameter and μ represents the dynamic viscosity of the sealing fluid and Q is the mass leakage rate.

The equation for the film thickness at any location, h(x) can be expressed as:

$$h(x) = h_c(x) + e\cos(\theta) \quad \text{..... (30)}$$

where e is the eccentricity, cos (θ) takes account of the angular values and $h_c(x)$ is the film thickness at the center of the clearance region which is basically the sum of the original film thickness and the elastic deformations along the region.

2.8 Lame's equation

Lame's equation is used to determine the maximum stresses which could be either hoop, radial or axial stresses in a thick-walled cylinder. The parameter, $h_c(x)$ can be obtained by using Lame's formula derived for a thick-walled cylinder:

$$h_c(x) = h_0\,(1 + k_1 p - k_2 p_0) \quad \text{..... (31)}$$

where p_0 is the working pressure, h_0 is the initial clearance and k_1 & k_2 represent the effect coefficients. The equation for determining k_1 and k_2 is expressed as:

$k_1 = k_2 = \frac{1}{Eh_0} \cdot \frac{DD_0^2}{D_0^2 - D^2}$ ..... (32)

where D_0 and D represent the external and internal diameters respectively, E is the Young's modulus and h_0 is the initial clearance

2.9 Dowson-Higginson formula

The relationship between the pressure and density is defined by the Dowson-Higginson formula:

$\rho = \rho_0 \left(1 + \frac{0.6p}{1+1.7p}\right)$ ..... (33)

where ρ_0 is the density of the fluid at atmospheric pressure and p is the working pressure.

2.10 Barus equation

The relationship between the pressure and viscosity is given by the Barus equation:

$\mu = \mu_0 \exp(\alpha p)$ ..... (34)

where μ_0 is the dynamic viscosity of the fluid at atmospheric pressure, α is the pressure-viscosity coefficient and p represent the pressure.

2.11 Dimensionless parameters

Dimensionless parameters would be introduced to help make the variables have scalar units or a unit with a ratio of 1. One of the most common dimensionless equations used in fluid flow problems is the Reynolds number which is different from the Reynolds equation we have above. The Reynolds number as known, is the ratio of inertial forces to viscous forces. In this case, the dimensionless parameters would be found for the Reynolds equation, Dowson-Higginson formula

and Barus equation. Dimensionless parameters are expressed with an overline. First, the dimensionless terms are defined as follows:

$$\bar{x} = \frac{x}{X} \quad \text{(35)}$$

$$\bar{y} = \frac{y}{Y} \quad \text{(36)}$$

$$\bar{z} = \frac{z}{Z} \quad \text{(37)}$$

$$\bar{h} = \frac{h}{h_0} \quad \text{(38)}$$

$$\bar{\rho} = \frac{\rho}{\rho_0} \quad \text{(39)}$$

$$\bar{\mu} = \frac{\mu}{\mu_0} \quad \text{(40)}$$

$$\bar{p} = \frac{p}{p_0} \quad \text{(41)}$$

$$\bar{k} = \frac{k}{k_0} \quad \text{(42)}$$

where X, Y, Z are the characteristic lengths in the x, y and z directions, h_0 is the characteristic film thickness, ρ_0 is the characteristic density, μ_0 is the characteristic viscosity, p_0 is the characteristic pressure and k_0 is the characteristic clearance coefficient. Substituting these dimensionless terms into the Reynolds equation, Dowson-Higginson formula and Barus equation, the resulting equations in dimensionless form can be expressed as:

$$\bar{Q} = \frac{(\overline{h_c(x)} + e\cos(\theta))^3\,\bar{p}}{\bar{u}}\,\frac{d\bar{p}}{d\bar{x}} \quad \text{(43)}$$

where

$\mu = \exp(\overline{\alpha p})$ ..... (44)

$\bar{\rho} = 1 + \frac{0.6\bar{p}p_0}{1+1.7\bar{p}p_0}$ ..... (45)

$\overline{h_c(x)} = 1 + \overline{k_1 p} - \overline{k_2}$ ..... (46)

$\left(\frac{h_0}{D}\right)\overline{k_1} = \left(\frac{h_0}{D}\right)\overline{k_2} = \frac{1}{\bar{E}}\frac{D_0/D}{(D_0/D)^2-1}$ ..... (47)

CHAPTER 3

METHODOLOGY

3.1. Elasto-hydrodynamic Seal Design

The proposed seal design would use the same elasto-hydrodynamic lubrication mechanism as explained in the case of journal bearing in Chapter 2.6. The EHD seal is attached to a back ring as shown in Figure 6 below with a length of 26.035mm and a thickness of 0.5mm. The stator is basically the housing which is a stationary component that houses the rotating shaft while the back ring attaches the seal to the stator. During stationary condition when the velocity is equal to 0, the seal sits horizontally on the rotor at a height of 0.05mm with no pressure exerted on it.

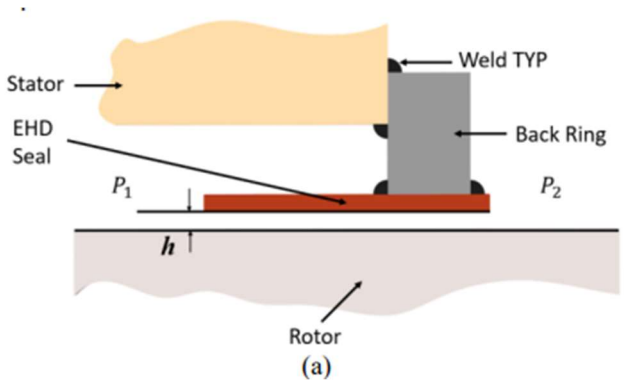

Figure 6: EHD Seal in Stationary Condition

When the system is started up and the velocity is greater than 0, the initial pressure P_1 is greater than the exit pressure P_2. (P_1>P_2) in the clearance region between the rotor and seal because the exit pressure P_2 would basically be the atmospheric pressure and the temperature at P_1 would be greater than at P_2 which also has a positive correlation with the pressure. P_1 exerts a uniformly distributed pressure at the top or upper face of the seal because no flow is exiting the system whereas at the bottom because P_1 is greater than P_2, the pressure exerted decreases from left to right. Due to the uniform pressure at the top and the decreasing pressure at the bottom, it causes

the seal to deform downwards eventually creating a throat in the clearance region. The throat is the point with minimum clearance or the point on the seal with the largest deformation. This thesis would be analyzing this deformation and pressure distribution using numerical solutions with MATLAB. Since the Reynolds equation and Lame's formula are both differential equations, the function ODE45 would be used to solve the differential equations and plot the graphs of the pressure and deformation to show their distribution on the seal with different working and initial pressures.

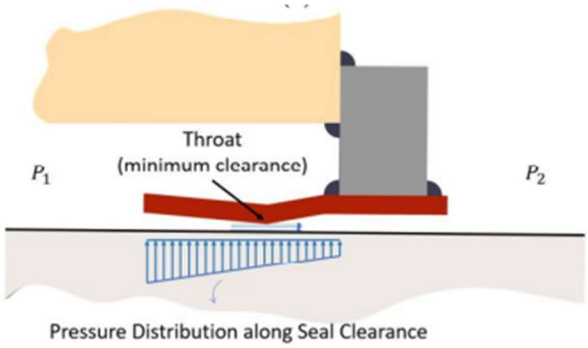

Figure 7: EHD Seal in Non-Stationary Condition

3.2 Model Geometry and Dimensions

The Figure 8 below shows the model geometry and dimensions of the EHD seal

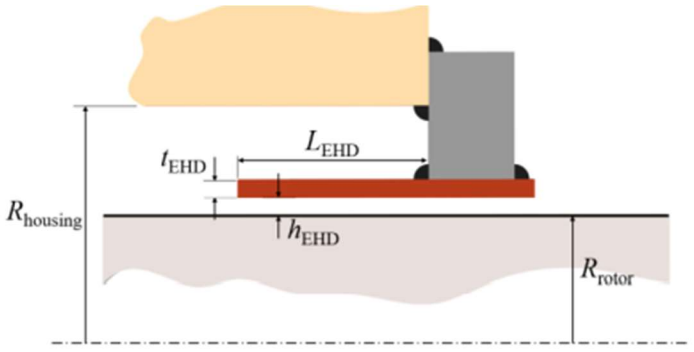

L_{EHD} = 26.035 mm | t_{EHD} = 0.5 mm | h_{EHD} = 0.05 mm | R_{rotor} = 25.4 mm | $R_{housing}$ = 50.8 mm

Figure 8: Model Geometry and Dimensions

where L_{EHD} is the length of the seal, t_{EHD} is the thickness of the seal, h_{EHD} is the height of the seal, R_{rotor} is the radius of the rotor and $R_{housing}$ is the radius of the housing.

3.3 Boundary Conditions

Regarding the boundary conditions, the properties of steel was selected with a Young's modulus and density of 200GPa and 876kg/m^3 respectively. Using the Barus equation, the pressure viscosity coefficient was found to be 0.0134e-6. The inlet pressure (P_{in}) started off at 2MPa but is modified to take account of the entire operation range while the outlet pressure (P_{out}) is set to be the atmospheric pressure. The $P_{calculated}$ at X=L should be equal to the atmospheric pressure that is:

$$P_{calculated\ X=L} = P_{out} = P_{atm} \quad \text{..... (48)}$$

3.4 Numerical Solution Procedure

To begin, the operation and material parameters of the seal are identified and listed out. From the Equation 29 shown above, the equation is highly non-linear and contains a differential equation term as the pressure being a function of the location. Equation 29 simply means that by multiplying the seal properties with the pressure gradient at any location in the seal would equal to the mass leakage rate, Q making the equation contain two unknown variables needed to be solved for, the pressure & mass leakage rate. This is where a differential solver tool would be required to solve the equations and MATLAB would be used in this case. To proceed, a logical value of Q is first assumed, and the differential equation is solved by using the ode45 function in MATLAB to determine the value of $P_{calculated}$ (Pressure). Ode45 function would be explained in Section 3.5. The $P_{calculated}$ is checked with the boundary condition in Eq (48). If the boundary condition is satisfied, a good guess of Q was made and does not need to be changed but if the

boundary condition is not satisfied, the value of Q is changed, and another iteration is performed until $P_{calculated}$ satisfies the boundary condition. This is the portion where if statements are used in the MATLAB code. Reasonable guesses of Q have to be chosen to avoid obtaining negative pressures from the solution which can lead to convergence problems and could take up a lot of computational time. The full written MATLAB code can be seen in the Appendix section of the thesis.

3.5 ODE45 Function

ODE45 is one of the more commonly used differential solvers to tackle ODE problems in MATLAB. It works well on most ODE problems and should be one of the first solvers that should be first tried when solving differential equations but if the problem requires a high accuracy other ODE solver like ode78, ode89, ode113 could be better suited for the problem. It uses the Runge-Kutta method that contains a dependent and independent variable and for this case the variables would be pressure (p) and location (x) would take the form:

$$\frac{dp}{dx} = f(x,p) \quad \text{..... (49)}$$

where x (location) is the independent variable, p (pressure) is the dependent variable and f (x, p) is a function in terms of x and p.

In MATLAB, it is coded under the format:

[x, p] = ode45(fname, xspan, y0, options)

where:

fname: is the name of the MATLAB .mfile that contains the function needed to be solved for,

xspan: sets the starting and ending limits of the integration [x0 xf]. It also sets the interval for the length steps if required by the user.

y0: sets the initial conditions for the solution

options: is a set of built-in integration settings that help increase accuracy when solving the ODE. It uses the ‘odeset’ function to pass an argument that can specify boundary values. Figure 9 shows the list of some of the existing options structure that can be set to have specified values instead of the default values.

```
          AbsTol
             BDF
          Events
      InitialStep
         Jacobian
        JConstant
         JPattern
             Mass
    MassSingular
        MaxOrder
         MaxStep
     NonNegative
     NormControl
       OutputFcn
       OutputSel
          Refine
          RelTol
           Stats
      Vectorized
MStateDependence
        MvPattern
    InitialSlope
```

Figure 9: MATLAB existing options structure list

In this case, only the AbsTol and RelTol would be modified to have specific values. The RelTol and AbsTol represents the relative and absolute tolerance respectively. RelTol is set to 1e-2 and AbsTol is set to 1e-5

CHAPTER 4

RESULTS AND DISCUSSION

4.1 Analytical Results and Discussion

The analytical results produced by the ODE solver would be discussed in this Chapter. Pressure Distribution, Clearance Distribution, Mass flow rate relating to the operating pressure are going to be analyzed to see how they affect the operation and performance of the seal. The working pressures would be evaluated from 0.2 MPa to 20 MPa with 10-time steps. 0.001kg/s would be used as the assumed mass flow rate Q, value to solve for the exit pressure. The material parameters & properties used in this work can be seen in Table 2 below.

Table 2: Material Parameters and Properties

Parameter	**Input data**
Dynamic viscosity (μ)	0.2177 kg/m·s
Pressure-viscosity coefficient (α)	0.0134e-6 1/Pa
Density of fluid (ρ)	876 kg/m^3
Young's Modulus (E)	214GPa
Diameter of the shaft (d_{shaft})	0.05008m
Thickness of the seal (t_{seal})	0.0005m
Length of the seal (L_{seal})	0.0265m
Mass flow rate (Q)	0.001kg/s
Initial seal clearance (h_0)	0.00005m
Internal diameter (D)	0.0502m
External diameter (D_0)	0.0509m

Outlet pressure (p_{out})	101,325 Pa
Number of iterations (N)	10,000

4.2 Pressure Distribution

Figure 10 portrays the Distance (x) vs Pressure plot of the seal depicting the pressure distribution as it moves from x=0 to x=L for operating pressure ranging from 0.2 MPa to 20 MPa. At lower operating pressures (P_0 < 7 MPa), the pressure decreases almost linearly along the location (x) but as the operating pressure increases it tends to decrease faster towards the end.

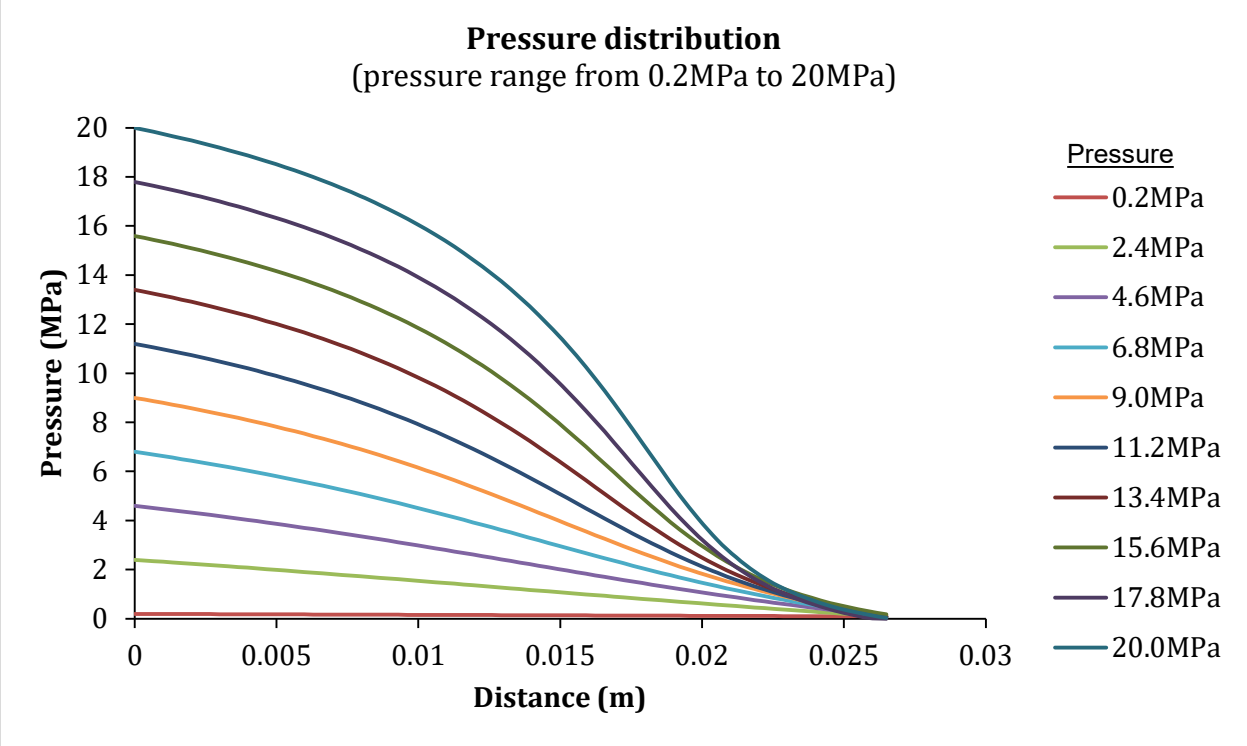

Figure 10: Pressure distribution plot from 0.2MPa to 20MPa

Table 3: Pressure at the mid-length location of the seal clearance (0.1325m)

Initial operating pressure (MPa)	Mid-length location of the seal (m)	Pressure at mid location (MPa)	% of pressure lost from the initial
0.2	0.1325	0.1477	26.15%
2.4	0.1325	1.2416	48.26%
4.6	0.1325	2.3549	48.80%
6.8	0.1325	3.5138	48.32%
9.0	0.1325	4.7738	46.95%
11.2	0.1325	6.1567	45.02%
13.4	0.1325	7.7437	42.21%
15.6	0.1325	9.5199	38.97%
17.8	0.1325	11.3938	35.98%
20.0	0.1325	13.4267	32.86%

The pressure distribution at the mid-length location of the seal before it reaches the exit (i.e., Atmospheric pressure) is shown in Table 3. Since the total length of the seal is 0.0265m, the mid-point location is determined to be 0.1325m. An interesting trend is seen from the amount of pressure lost from the initial operating pressure. The % of pressure lost from initial decreases as the initial operating pressure increases except from the 0.2 MPa which can be explained by the fact that it is close to the atmospheric pressure (0.1013MPa) meaning there is not much of pressure variation from the start to the end point. It's a good way to predict around which location the elastic deformation of the seal starts to occur. For example, 20MPa loses about 33% of its initial pressure at the mid location so it would be reasonable to say that the elastic deformation starts to occur

around this region and the throat slightly pass the mid-point due to the pressure drop (67%) that would happen close to the end location at atmospheric pressure.

4.3 Clearance Distribution

Clearance (h) vs distance (x) plot, shown in Figure 11, depicts the elastic deformation of the seal as it moves from x=0 to x=L for operating pressure ranging from 0.2 MPa to 20 MPa. At higher pressures, the seal deforms more because more force is acting on the seal compared to lower pressures which explains why the throat (minimum clearance) is the lowest at the highest pressure (20MPa). When the pressure is applied, the seal clearance starts off as 50μm at x=0 and the seal start to bend as pressure passes through it until it reaches its bending limit at a certain location. This can be called the throat location. This is the location where the seal attains its minimum clearance area.

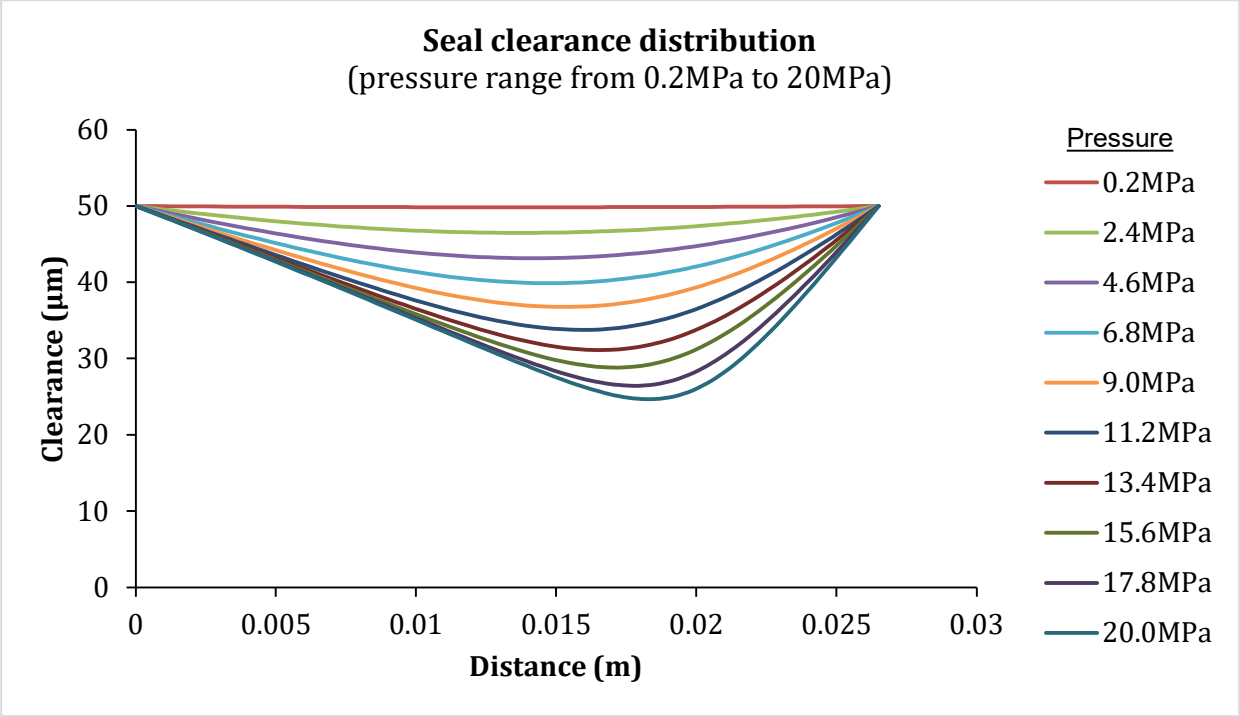

Figure 11: Seal clearance distribution plot from 0.2MPa to 20MPa

Table 4: Seal clearance at throat location

Initial operating pressure (MPa)	**Initial seal clearance (h_0)**	**Clearance height at throat (h_t)**	**% of original shape lost at h_t (Elasticity limit)**	**Throat location (h_x)**
0.2	50.0µm	49.8µm	0.4%	0.012588m
2.4	50.0µm	46.5µm	7%	0.01325m
4.6	50.0µm	43.2µm	13.6%	0.013913m
6.8	50.0µm	39.9µm	20.2%	0.014575m
9.0	50.0µm	36.8µm	26.4%	0.015238m
11.2	50.0µm	33.8µm	32.4%	0.01590m
13.4	50.0µm	31.1µm	37.8%	0.016563m
15.6	50.0µm	28.8µm	42.4%	0.017225m
17.8	50.0µm	26.4µm	47.2%	0.017888m
20	50.0µm	24.7µm	50.6%	0.01855m

The clearance height and location at the throat region of the seal for different operating pressures is depicted in Table 4 above. The trend depicts that as the operating pressure rises the clearance height at the throat (h_t) decreases and the location (x) of the throat increases further down the length of the seal. This means that as the operator continues to apply more pressure, the velocity also increases and causes the seal continues to deform more and more along its length thereby decreasing the clearance height from the initial. Since the total length of the seal is 0.02650m, it is reasonable to say that at higher pressures the throat occurs closer to the end of the seal. The seal has a high elasticity limit because the material used is steel which has an elasticity of 214GPa and would be capable of withstanding high pressures as the pressure increases compared to the other

materials used for other sealing technologies shown in Table 1. The seal would deform without failing, losing more than half of its original shape (50.6%) at throat position (20.5μm) when pressure is 20MPa compared to x=0 when the clearance is 50μm. Applying pressures higher than this could make the seal fail in real life applications because permanent deformation could occur if it stresses exceeds the elasticity limit by continuous losing more % of its original shape. MATLAB code for pressures higher than 25-30MPa generates error messages which indicates that compressibility effect of the fluid at the throat location cannot ignored at a very high pressure

4.4 Mass Flow Rate

The mass flow rate vs pressure plot for initial operating pressure ranging from 0.2 MPa to 20 MPa is shown in Figure 12. At low operating pressures, the mass flow rate increases linearly as the pressure increases because at this stage the seal is subjected to little or no elastic deformation therefore there is barely any change in its cross-sectional flow area. However, with increasing pressure at the high-pressure limit, mass flow rate plateaued. The pressure continues to rise until it reaches a point where it would be subject to deformation and the flow surface area would reduce and from the given mass flow rate equation = ρVA the area is directly proportional to the mass flow rate. This explains the bending curve on the graph and why the mass flow rate doesn't continue to rise linearly all the way as the pressure increases. At much higher pressures, the mass flow rate is smaller compared to lower pressures and this is a desirable attribute for seals to have because a smaller mass flow rate = smaller leakage.

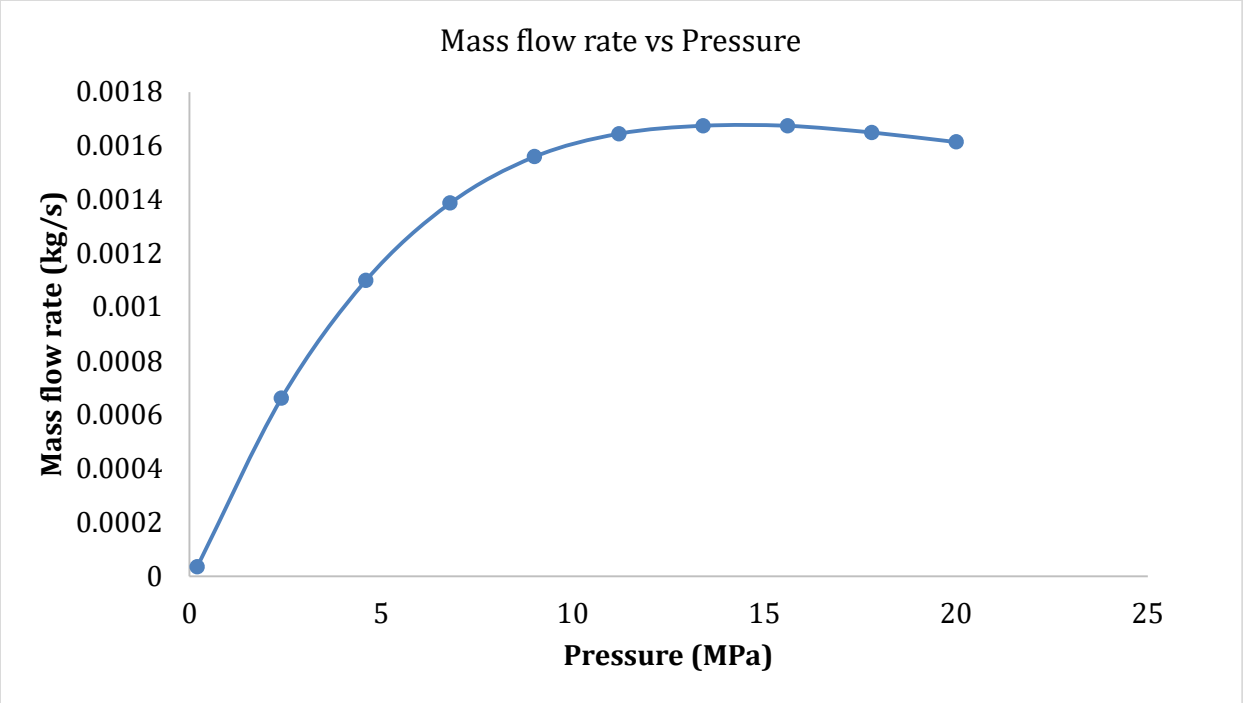

Figure 12: Mass flow rate (kg/s) vs Pressure (Pa) plot

Table 5: Mass flow rate values at different operating pressures

Initial operating pressure (MPa)	Mass flow rate, Q (kg/s)
0.2	3.50E-05
2.4	0.00063
4.6	0.0011
6.8	0.001387
9.0	0.00156
11.2	0.001645
13.4	0.001675
15.6	0.001675
17.8	0.00165

20.0	0.001615

The Mass flow rate (Q) values for different operating pressures can be seen in Table 5 above. From the Table, at 13.4MPa the mass flow rate begins to decrease as the pressure increased. It would be safe to say that the deformation of the seal would start to occur close to/around that pressure owing to the reduction in the mass flow rate. A smaller mass flow rate at higher pressures would always be an advantageous feature for a seal to possess.

4.5 Parametric Study

In order to achieve the primary goal of a low leakage rate, a parametric study was carried out to see how much influence/effect changing a certain input parameter or property of the seal would have on the clearance distribution and the mass flow rate graphs. The parameters that were studied include: seal thickness, diameter of the shaft and the seal length at a low, intermediate and high pressure of 5MPa, 10MPa and 20MPa. The seal thickness was analyzed for the range: 0.5mm – 2mm.The diameter of the shaft was analyzed for the range: 25.08mm – 50. 08mm.The seal length was analyzed for the range: 13mm – 28mm.The results showed that altering an input design geometry or property of the seal plays a huge role in the performance and leakage of the seal. The analysis would be explained in detail below. These input parameters and their respective ranges can be found in Table 6 below.

Table 6: Geometric parameters for the parametric study

Parameters	**Design parameter**	**Values for parametric study**
Seal thickness	0.38485mm	0.5, 0.75, 1.0, 1.25, 1.5, 2.0 mm

Shaft diameter	50.08mm	25.08, 30.08, 35.08, 40.08, 45.08, 50.08 mm
Seal length	26.50mm	13, 18, 23, 28mm

4.5.1 Varying seal thickness

The thickness of the seal is a very important property to consider during the design stage of a seal. A seal that is not thick enough for the job would be very flimsy and would fail easily and a seal that is too thick would not be able to deform easily to account for higher pressures so getting the right seal thickness for the job could be tricky. For this study, the seal thickness was modified for the range: 0.5mm to 2mm to see and compare the differences between a thinner and thicker seal with relation to seal clearance distribution and mass flow rate.

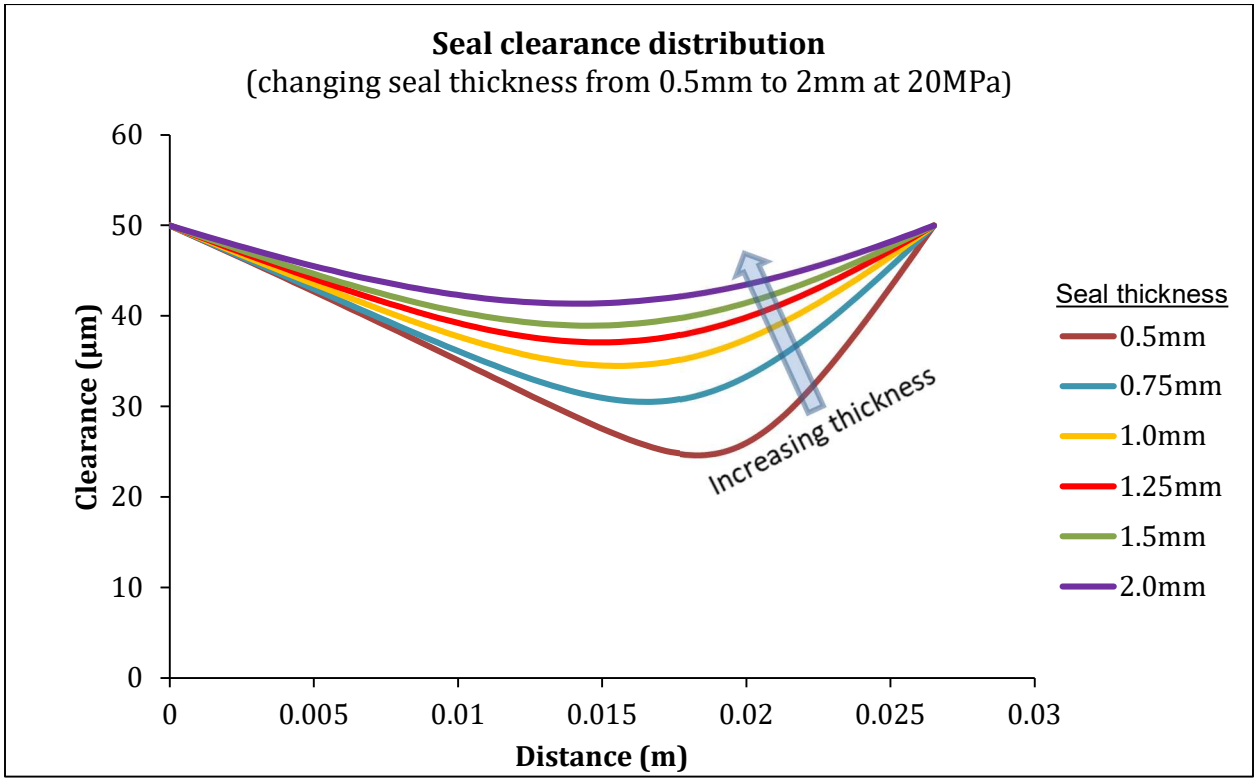

Figure 13: Clearance distribution graph by varying the seal thickness at high pressure (20MPa)

From Figure 13, the smallest seal thickness (0.5mm) in this case produced the lowest throat/clearance value which is logical because a thinner object would deform much easier than a thicker object when subject to the same pressure. Sealing would be more desirable with a thinner seal but the amount of pressure to be applied and the diameter of the shaft should be taken into consideration when selecting the thickness of the seal.

Table 7: Throat values for varying seal thickness at 20MPa

Seal thickness	**Initial pressure**	**Throat height (h_t)**	**% of original height lost at h_t**	**Throat location (h_x)**
0.5mm	20MPa	24.7µm	50.6%	0.01855m
0.75mm	20MPa	30.5µm	39.0%	0.01656m
1.0mm	20MPa	34.5µm	31%	0.01523m
1.25mm	20MPa	37.1µm	25.8%	0.01458m
1.5mm	20MPa	39.0µm	22%	0.01458m
2.0mm	20MPa	41.4µm	17.2%	0.01325m

The Throat height and location that is where there is minimum clearance between the shaft and the seal for different seal thickness at 20MPa is shown in Table 7. As the seal thickness increases, the throat height increases, and the throat location moves towards the left. The minimum and maximum throat height are 24.7µm and 41.4µm respectively. A difference in throat height of 16.7µm.

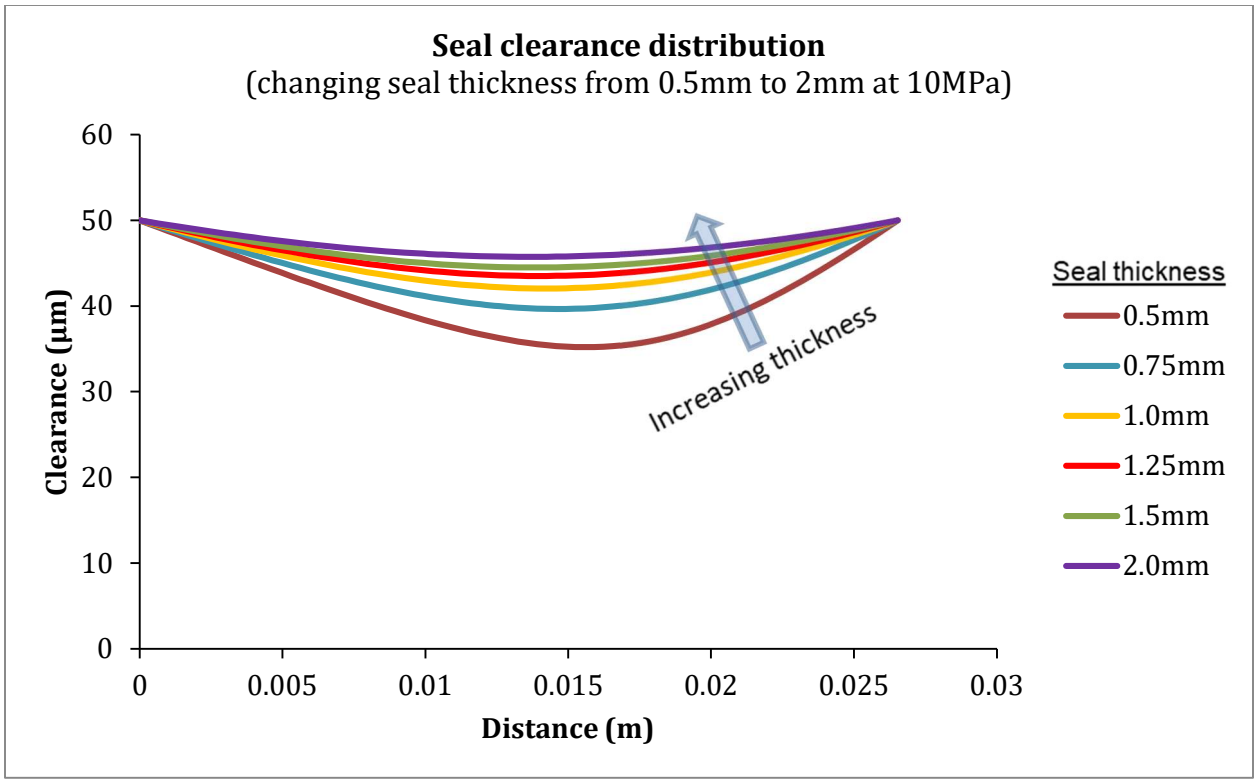

Figure 14: Clearance distribution graph by varying the seal thickness at intermediate pressure (10MPa)

A similar trend is shown in Figure 14 with Figure 13 except that the clearance becomes bigger for the same seal thickness to account for the reduction in pressure (10MPa).

Table 8: Throat values for varying seal thickness at 10MPa

Seal thickness	**Initial pressure**	**Throat height (h_t)**	**% of original height lost at h_t**	**Throat location (h_x)**
0.5mm	10MPa	35.2µm	29.6%	0.01524m
0.75mm	10MPa	39.7µm	20.6%	0.01458m
1.0mm	10MPa	42.1µm	15.8%	0.01391m
1.25mm	10MPa	43.5µm	13%	0.01391m
1.5mm	10MPa	44.5µm	11%	0.01391m
2.0mm	10MPa	45.8µm	8.4%	0.01259m

The Throat values at an intermediate pressure of 10MPa is depicted in Table 8. It is interesting to note that throat location for the 0.5mm seal thickness (0.01524m) at 10MPa is about the same for a 1.0mm seal thickness at 20MPa and 0.75mm seal thickness throat location at 10MPa is about the same for that of 1.25mm and 1.50mm at 20MPa. The minimum and maximum throat height are 35.2µm and 45.8µm respectively. A difference in throat height of 10.6µm.

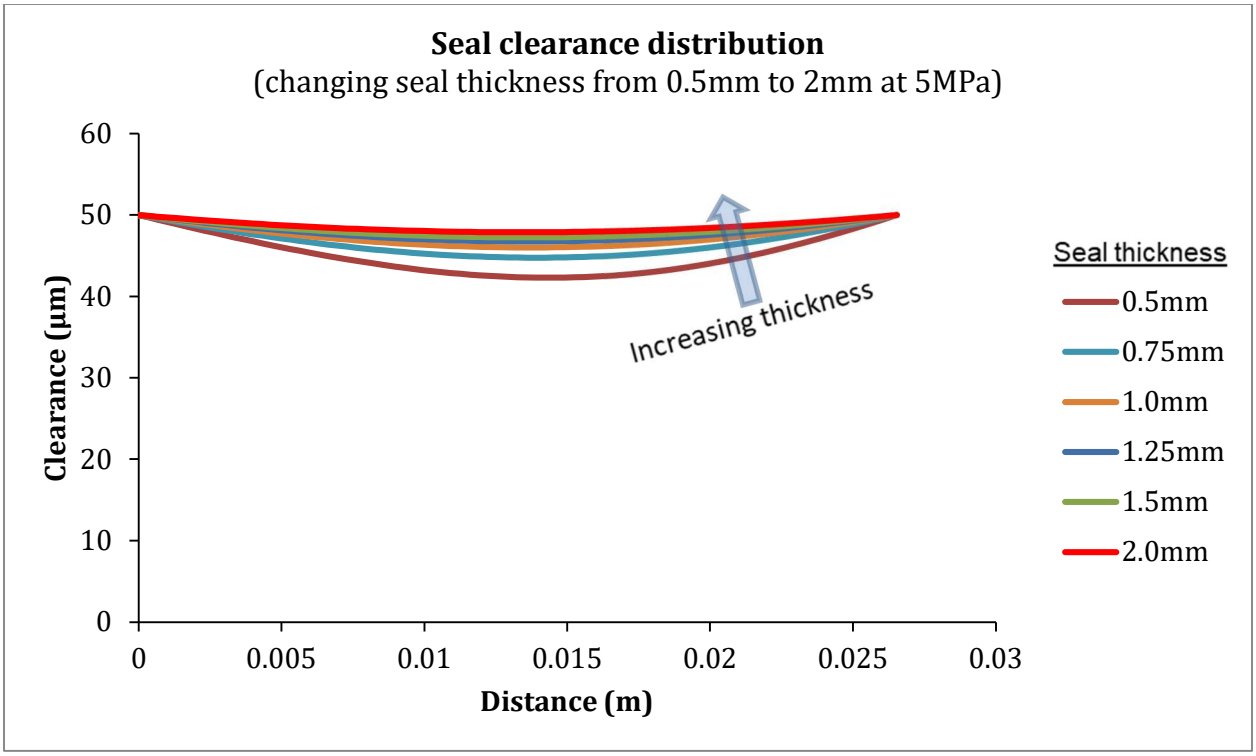

Figure 15: Clearance distribution graph by varying the seal thickness at a low pressure (5MPa)

A similar trend is illustrated in Figure 15 with that of Figure 13 and Figure 14, the seal with the least thickness produced the most elastic deformation or minimum clearance and vice versa.

Table 9: Throat values for varying seal thickness at 5MPa

Seal thickness	**Initial pressure**	**Throat height (h_t)**	**% of original height lost at h_t**	**Throat location (h_x)**
0.5mm	5MPa	42.3µm	15.4%	0.01420m
0.75mm	5MPa	44.8µm	10.4%	0.01390m

1.0mm	5MPa	46.0µm	8.0%	0.01325m
1.25mm	5MPa	46.8µm	6.4%	0.01259m
1.5mm	5MPa	47.3µm	5.4%	0.01193m
2.0mm	5MPa	47.9µm	4.2%	0.01126m

The Throat values at a low pressure of 5MPa is portrayed in Table 9 above. No surprises here from Table 8, at a much lower pressure the deformation of the seal would also be lower which explains the higher throat height gotten compared with Table 7 and Table 8. The difference in throat height from 0.5mm to 2mm was also the least with a difference of 5.6µm.

Table 10: Min and max throat values at different initial pressures when varying seal thickness

Initial pressure	**Min throat height at 0.5mm**	**Max throat height at 2.0mm**	**Difference (max throat - min throat)**
5MPa	42.3µm	47.9µm	5.6µm
10MPa	35.2µm	45.8µm	10.6µm
20MPa	24.7µm	41.4µm	16.7µm

It can be verified from Table 10 that as the pressure increases when varying the thickness, the elastic deformation also increases which explains why the difference in the max and min throat height also increases.

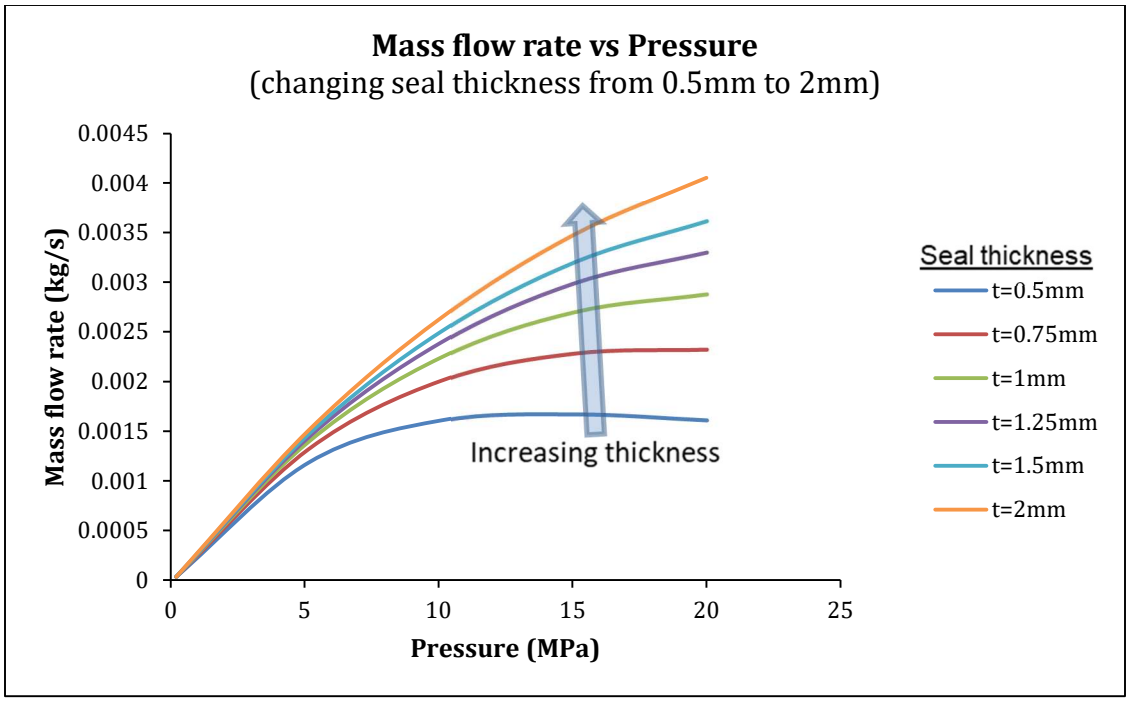

Figure 16: Mass flow rate vs Pressure plot with varying seal thickness

As seen in Figure 16, it can be verified that the seal with a lower thickness would produce a lower mass flow rate compared with that of a thicker one when subject to higher pressures. This is because at those higher pressures, the thinner seal would deform more as the shaft rotates faster. This deformation reduces the flow area and ultimately reducing the flow rate as the flow area is directly proportional to the flow rate from the equation $Q = \rho VA$. A seal with lower mass flow rate would also mean a lower leakage rate which is a quality of a good seal.

Table 11: Mass flow rate for varying seal thickness at 20MPa

Seal thickness	**Initial pressure**	**Mass flow rate**
0.5mm	20MPa	0.00161 kg/s
0.75mm	20MPa	0.00233 kg/s
1.0mm	20MPa	0.00288 kg/s
1.25mm	20MPa	0.00330 kg/s

1.5mm	20MPa	0.00361 kg/s
2.0mm	20MPa	0.004055 kg/s

Table 12: Mass flow rate for varying seal thickness at 10MPa

Seal thickness	**Initial pressure**	**Mass flow rate**
0.5mm	10MPa	0.00161 kg/s
0.75mm	10MPa	0.00201 kg/s
1.0mm	10MPa	0.00224 kg/s
1.25mm	10MPa	0.00239kg/s
1.5mm	10MPa	0.00250 kg/s
2.0mm	10MPa	0.00264 kg/s

Table 13: Mass flow rate for varying seal thickness at 5MPa

Seal thickness	**Initial pressure**	**Mass flow rate**
0.5mm	5MPa	0.00118 kg/s
0.75mm	5MPa	0.00132 kg/s
1.0mm	5MPa	0.00139 kg/s
1.25mm	5MPa	0.00144 kg/s
1.5mm	5MPa	0.00147 kg/s
2.0mm	5MPa	0.00151 kg/s

4.5.2 Varying shaft diameter

The diameter of the rotating shaft is another important parameter that could greatly influence the behavior or performance of the seal. A larger shaft diameter would mean a larger working surface area and vice versa. Naturally, a shaft with a smaller diameter would be more compact and harder to deform than that with a larger diameter. We would try and verify these statements in the analysis below. For this study, the diameter of the shaft was analyzed for the range: 25.08mm to 50.08mm.

Figure 17 below depicts the Clearance distribution graph by varying the shaft diameter at a high pressure of 20MPa.

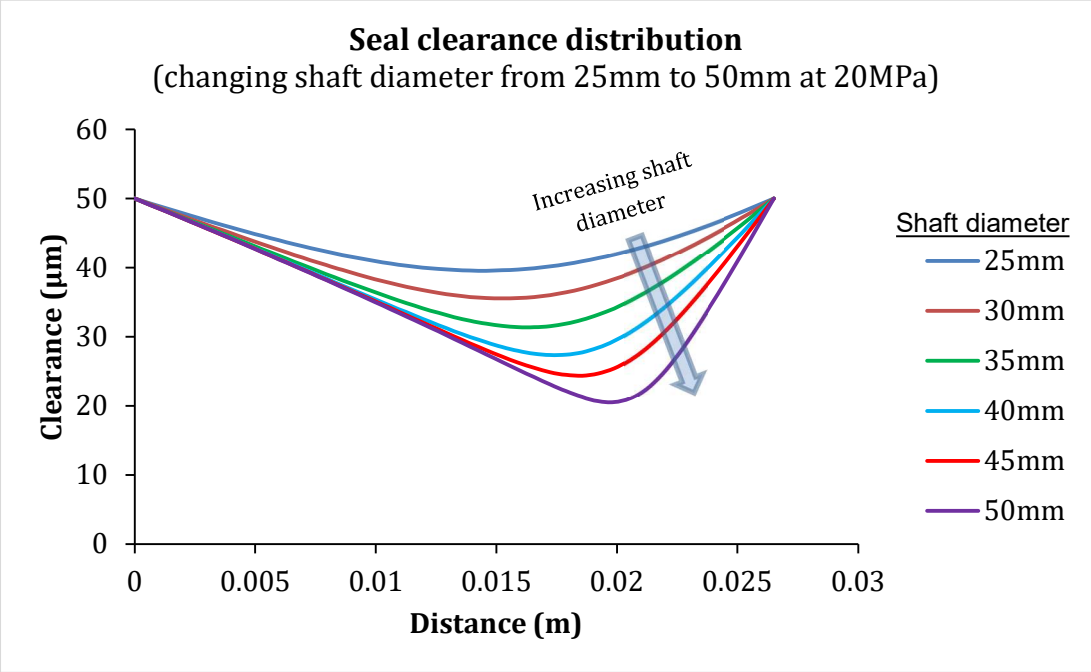

Figure 17: Clearance distribution graph by varying the shaft diameter at high pressure (20MPa)

As the shaft diameter increases, the clearance height decreases. This is particularly true because the shaft with a larger diameter is less compact and deforms more under higher pressures compared with than of a smaller shaft diameter. This explains the trend of the graph seen in Figure 17 above.

Table 14: Throat values for varying shaft diameter at 20MPa

Shaft diameter	**Initial pressure**	**Throat height (h_t)**	**% of original height lost at h_t**
25.08mm	20MPa	39.6µm	20.8%
30.08mm	20MPa	35.5µm	29.0%
35.08mm	20MPa	31.4µm	37.2%
40.08mm	20MPa	27.4µm	45.2%
45.08mm	20MPa	24.4µm	51.2%
50.08mm	20MPa	20.5µm	56.0%

The minimum clearance/throat values when the diameter of the shaft was varied from 25mm to 50mm at 20MPa is depicted in Table 14. The minimum and maximum throat heights are found to be 20.5µm and 39.6µm respectively. The difference between the max and min throat height is calculated to be 19.1µm. It can be deducted from the Table 14 that, for every time the shaft diameter increased by 5mm, the throat height decreased by about 4µm.

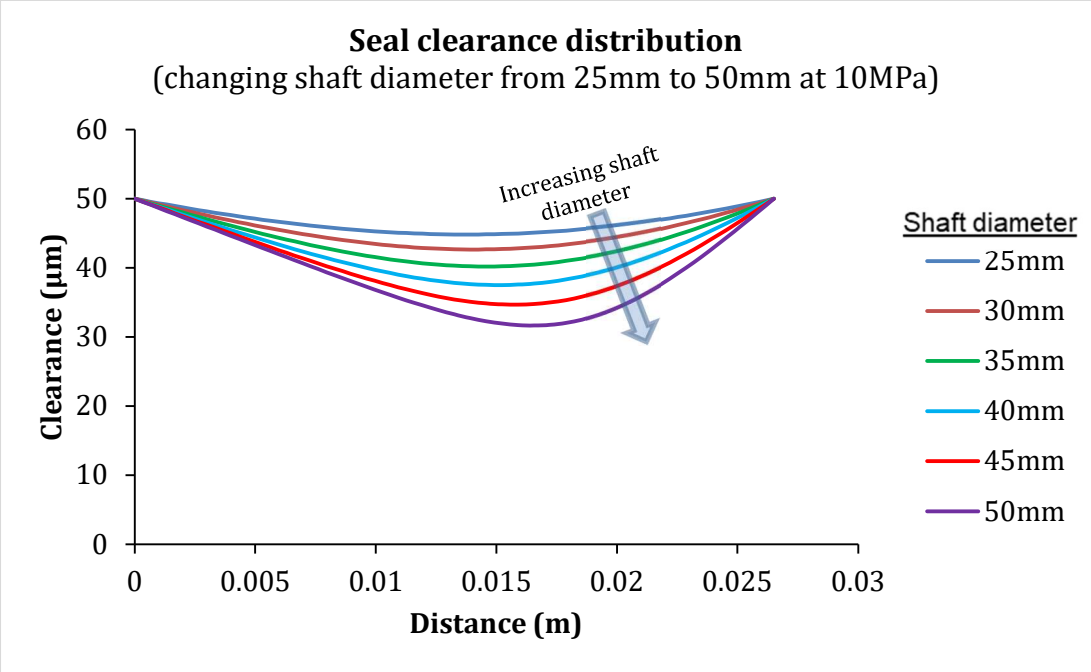

Figure 18: Clearance distribution graph by varying the shaft diameter at intermediate pressure (10MPa)

A similar trend is shown in Figure 18 with that of Figure 17 except that the clearance becomes bigger for the same shaft diameter to account for the reduction in pressure (10MPa).

Table 15: Throat values for varying shaft diameter at 10MPa

Shaft diameter	**Initial pressure**	**Throat height (h_t)**	**% of original height lost at h_t**
25.08mm	10MPa	44.8µm	10.4%
30.08mm	10MPa	42.7µm	14.6%
35.08mm	10MPa	40.2µm	19.6%
40.08mm	10MPa	37.5µm	25.0%
45.08mm	10MPa	34.7µm	30.6%
50.08mm	10MPa	31.7µm	36.6%

The Throat values when the diameter of the shaft was varied from 25mm to 50mm at an intermediate pressure of 10MPa is portrayed in Table 15. The minimum and maximum throat height are found to be 31.7µm and 44.8µm respectively. The difference between the max and min throat height is calculated to be 13.1µm.

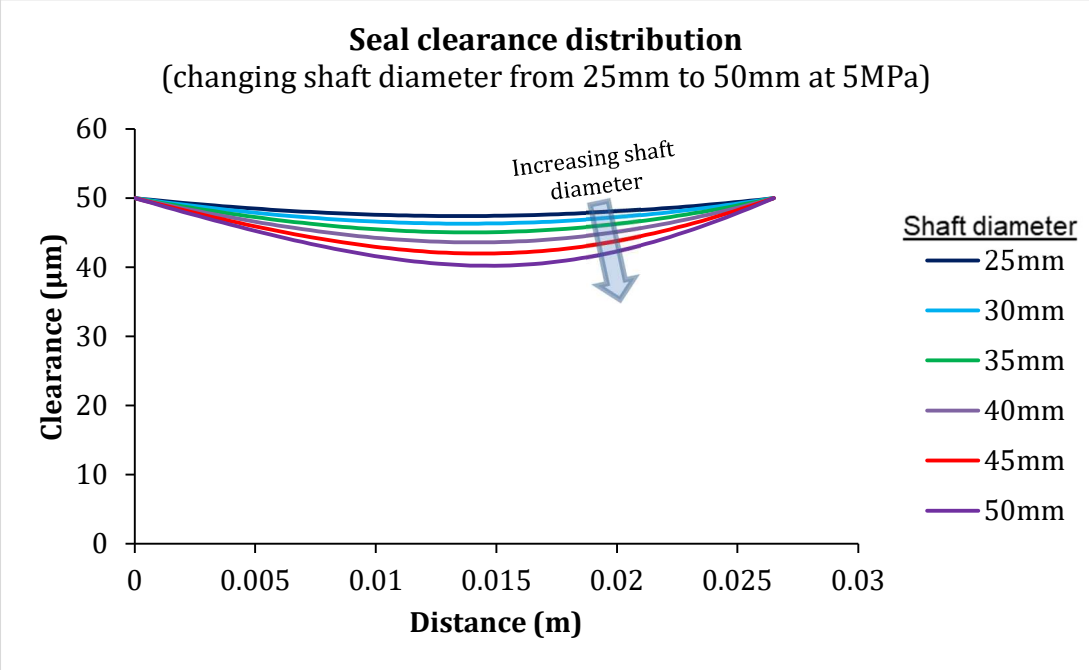

Figure 19: Clearance distribution graph by varying the shaft diameter at low pressure (5MPa)

By changing the pressure to 5MPa, the new clearance distribution graph was plotted when the diameter of the shaft was varied. The graph can be seen in Figure 19 above. The same trend is also shown like that of Figure 17 and Figure 18 which is as the shaft diameter increases, the clearance height decreases and vice versa.

Table 16: Throat values for varying shaft diameter at 5MPa

Shaft diameter	**Initial pressure**	**Throat height (h_t)**	**% of original height lost at h_t**
25.08mm	5MPa	47.4µm	5.2%
30.08mm	5MPa	46.3µm	7.4%
35.08mm	5MPa	45.0µm	10.0%

40.08mm	5MPa	43.6µm	12.8%
45.08mm	5MPa	42.0µm	16.0%
50.08mm	5MPa	40.2µm	9.6%

The Throat values gotten when the shaft diameter was varied from 25mm to 50mm at 5MPa is presented in Table 16. The minimum and maximum throat height are found to be 40.2µm and 47.4µm respectively. The difference between the minimum and maximum throat height is calculated to be 7.2µm.

Table 17: Min and max throat values at different initial pressures when varying shaft diameter

Initial pressure	Min throat height at 50.08mm	Max throat height at 25.08mm	Difference (|max throat - min throat|)
5Mpa	40.2µm	47.4µm	7.2µm
10MPa	31.7µm	44.8µm	13.1µm
20MPa	20.5µm	39.6µm	19.1µm

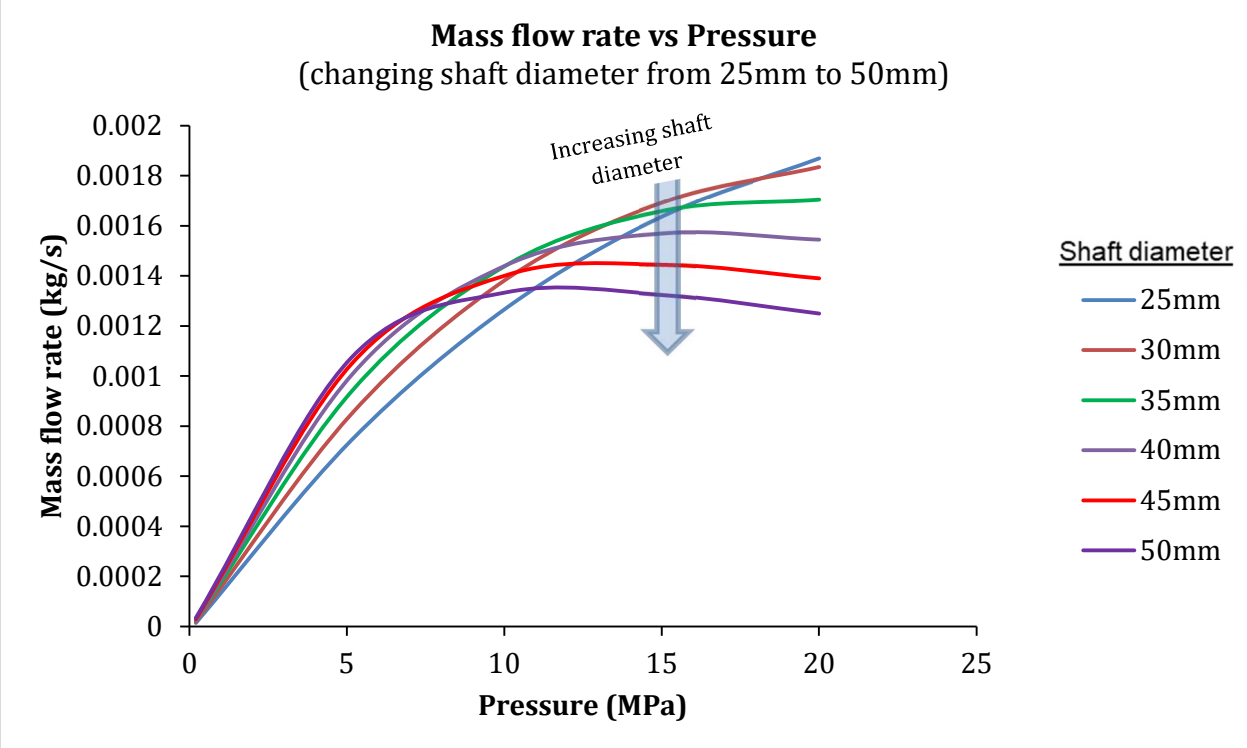

Figure 20: Mass flow rate vs Pressure plot with varying shaft diameter

The mass flow rate vs pressure plot when the shaft diameter is varied from 25.08mm to 50.08mm at 0.2 MPa to 20 MPa is presented in Figure 20. Initially, as the pressure and diameter of the shaft increases, the mass flow rate increases because a shaft with a larger diameter would naturally also have a larger area, and this has a positive correlation with the mass flow rate but as the pressure gets higher and higher, the mass flow rate tends to start decreasing with increasing shaft diameter because elastic deformation occurs at this stage and it alters the working surface area to decrease resulting in a decrease in the mass flow rate also. The higher the shaft diameter, the higher elastic deformation happens. Notice that at shaft diameter of 25mm the mass flow rate is slightly linear in shape sloping upwards, this is because the shaft has a smaller radius and is more compact in shape it would resist elastic deformation compared with a shaft diameter of 50mm at much higher pressures. Hence, the surface area would not be altered as much for the 25mm shaft diameter which means that the mass flow rate would continue to rise as the pressure rises until it reaches a pressure it can't withstand. As known, a good seal should have a low mass flow rate even when the pressure increases so ideally in this case a seal with a larger shaft diameter would be better to be selected.

Table 18: Mass flow rate for varying shaft diameter at 20MPa

Shaft diameter	**Initial pressure**	**Mass flow rate**
25mm	20MPa	0.00187 kg/s
30mm	20MPa	0.001835 kg/s
35mm	20MPa	0.001705 kg/s
40mm	20MPa	0.001545 kg/s
45mm	20MPa	0.00139 kg/s
50mm	20MPa	0.00125 kg/s

Table 19: Mass flow rate for varying shaft diameter at 10MPa

Shaft diameter	Initial pressure	Mass flow rate
25mm	10MPa	0.001275 kg/s
30mm	10MPa	0.00139 kg/s
35mm	10MPa	0.001445 kg/s
40mm	10MPa	0.001445 kg/s
45mm	10MPa	0.001405 kg/s
50mm	10MPa	0.001335 kg/s

Table 20: Mass flow rate for varying shaft diameter at 5MPa

Shaft diameter	Initial pressure	Mass flow rate
25mm	5MPa	0.000745 kg/s
30mm	5MPa	0.00085 kg/s
35mm	5MPa	0.00094 kg/s
40mm	5MPa	0.001005 kg/s
45mm	5MPa	0.00105 kg/s
50mm	5MPa	0.001075 kg/s

4.5.3 Varying seal length

The length of the seal is the final geometric parameter investigated to see the effect it has on the clearance and mass flow rate of the seal. Applying the laws of physics, a longer pipe would naturally take a longer time for the fluid flowing to reach the exit compared with a shorter pipe of the same diameter if the same pressure and velocity are applied. A parametric study is conducted

to see if similar behavior occurs for the proposed seal. The design seal length used for this model was 26.50mm. For this study, the seal length was analyzed for the range: 13mm to 28mm for 20MPa, 10MPa and 5MPa. Complete analysis done for the length of the seal is explained below.

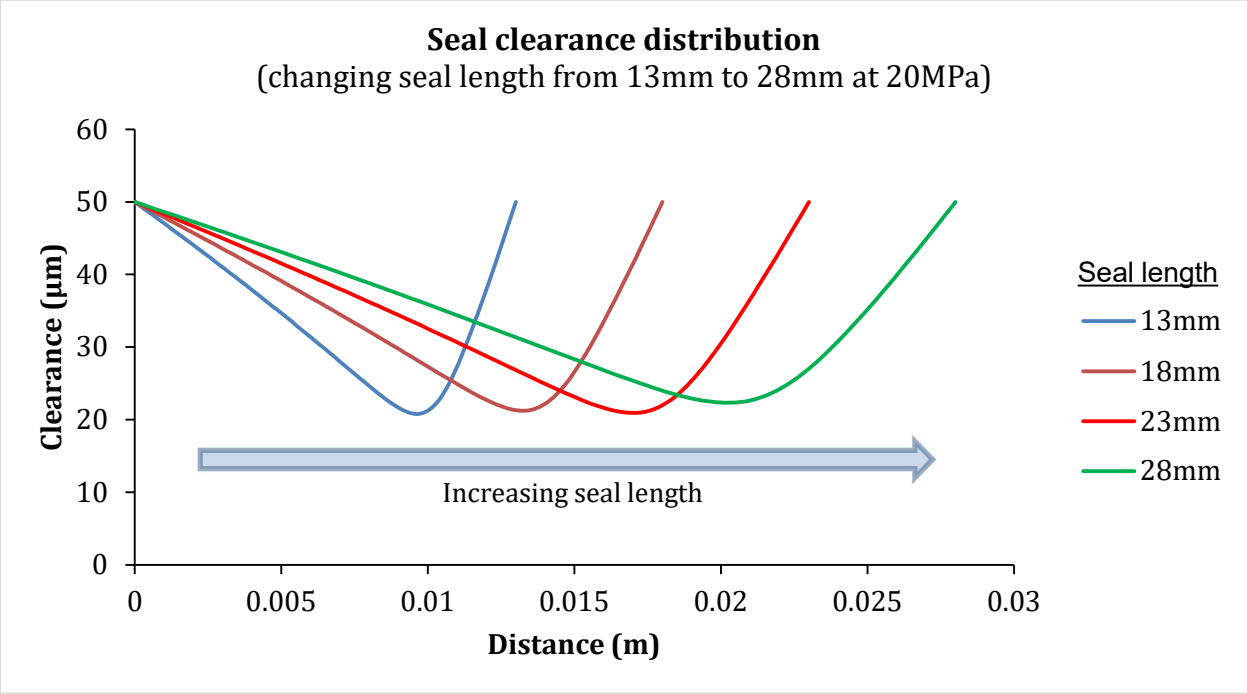

Figure 21: Clearance distribution graph by varying the seal length at high pressure (20MPa)

The graph of the seal clearance distribution when the seal length is varied at high pressure of 20MPa is illustrated in Figure 21 above. The minimum clearance/throat height came out to be relatively in the same range for all the seal lengths but the location it occurs at changes across the length for the different seal lengths. This comes as no surprise as one would expect the deformation to occur where the seal is highly choked or has the highest-pressure difference between P_2 and P_1, and this would occur at different locations for different seal lengths. It would not be a reasonable assumption to expect a seal with length 15mm to deform at the same location of that with a length of 28mm because the location where the 28mm long seal would attain its highest-pressure difference would be different of that of a 15mm long seal. It can be concluded from Figure 21 that

the thickness of the seal has a much greater influence on the clearance height and elastic deformation compared to the length of the seal.

Table 21: Throat values for varying seal length at 20MPa

Seal length	Initial pressure	Throat height (h_t)	% of original height lost at h_t	Throat location (h_x)
13mm	20MPa	20.8µm	58.4%	0.00975m
18mm	20MPa	21.3µm	57.4%	0.0135m
23mm	20MPa	21.7µm	56.5%	0.01725m
28mm	20MPa	22.3µm	55.4%	0.0203m

It can be verified in Table 21 that the seal length has little influence on the throat height (h_t) compared to the seal thickness and diameter of the shaft in Table 7 and Table 14 respectively. It produced less than a 1µm height difference as the seal length increment increased by 5mm. It can be confirmed again from Table 21 that the throat location would most likely occur slightly past the mid-point location of the seal.

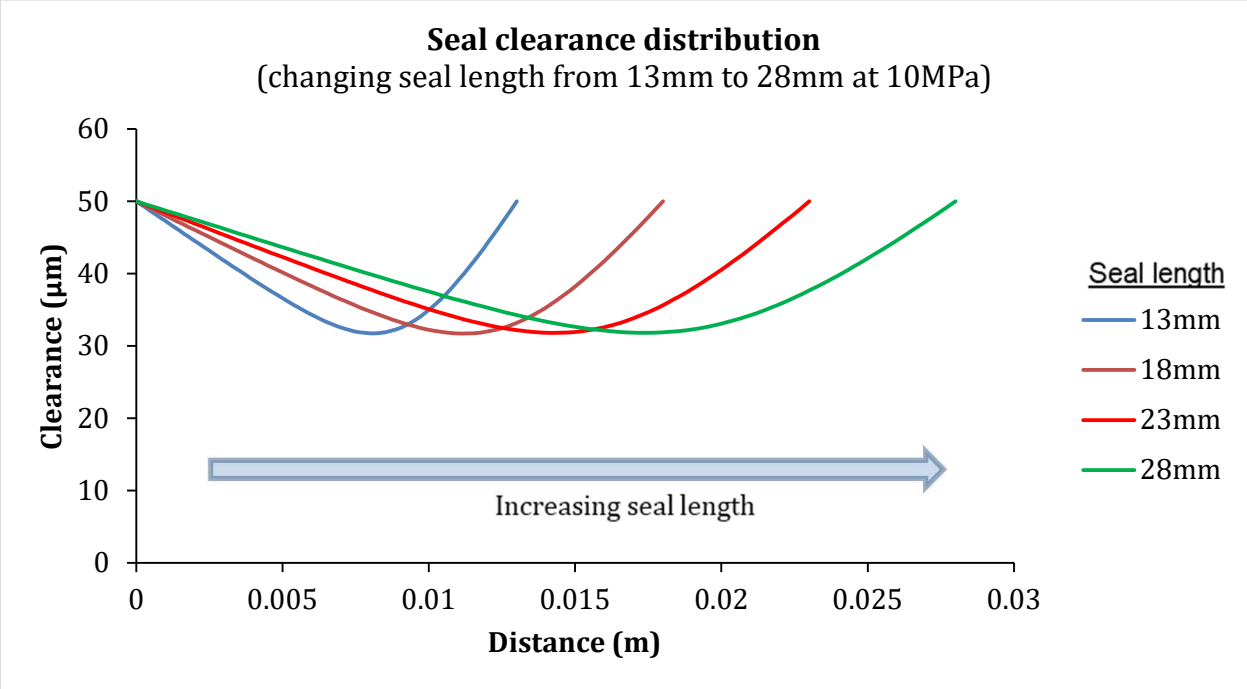

Figure 22: Clearance distribution graph by varying the seal length at intermediate pressure (10MPa)

Table 22: Throat values for varying seal length at 10MPa

Seal length	Initial pressure	Throat height (h_t)	% of original height lost at h_t	Throat location (h_x)
13mm	10MPa	31.8µm	36.4%	0.0078m
18mm	10MPa	31.8µm	36.4%	0.01125m
23mm	10MPa	31.8µm	36.4%	0.01438m
28mm	10MPa	31.8µm	36.4%	0.0175m

The throat location moves a little further away from the end of the seal and the throat height increases when the pressure is reduced to 10MPa. The throat height appears to remain constant for all 4 seal lengths at 31.8µm in Table 22.

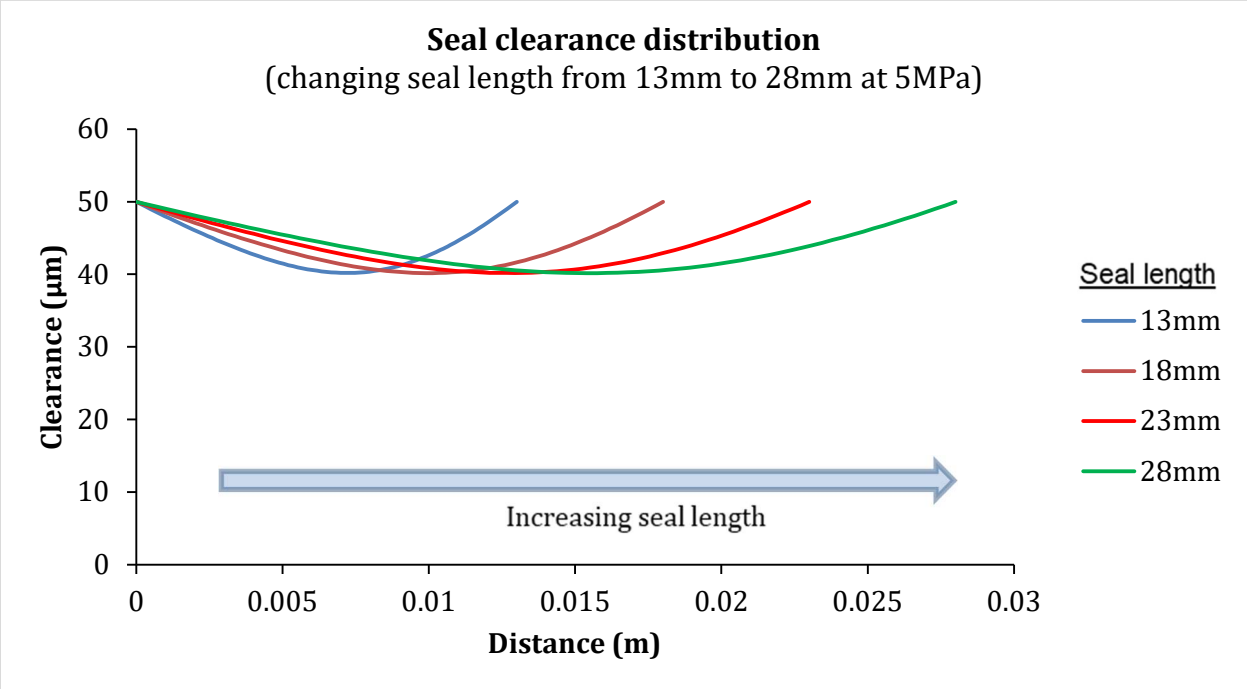

Figure 23: Clearance distribution graph by varying the seal length at intermediate pressure (5MPa)

Table 23: Throat values for varying seal length at 5MPa

Seal length	Initial pressure	Throat height (h_t)	% of original height lost at h_t	Throat location (h_x)
13mm	5MPa	40.2µm	19.6%	0.00715m
18mm	5MPa	40.2µm	19.6%	0.01035m
23mm	5MPa	40.2µm	19.6%	0.01323m
28mm	5MPa	40.2µm	19.6%	0.0161m

Similar trend seen for the throat height and location in Table 22 also occurs for Table 23.

Table 24: Min and max throat values at different initial pressures when varying seal length

Initial pressure	Min throat height at 13mm	Max throat height at 28mm	Difference (|max throat - min throat|)
5MPa	40.2µm	40.2µm	0µm
10MPa	31.8µm	31.8µm	0µm
20MPa	20.8µm	22.3µm	1.5µm

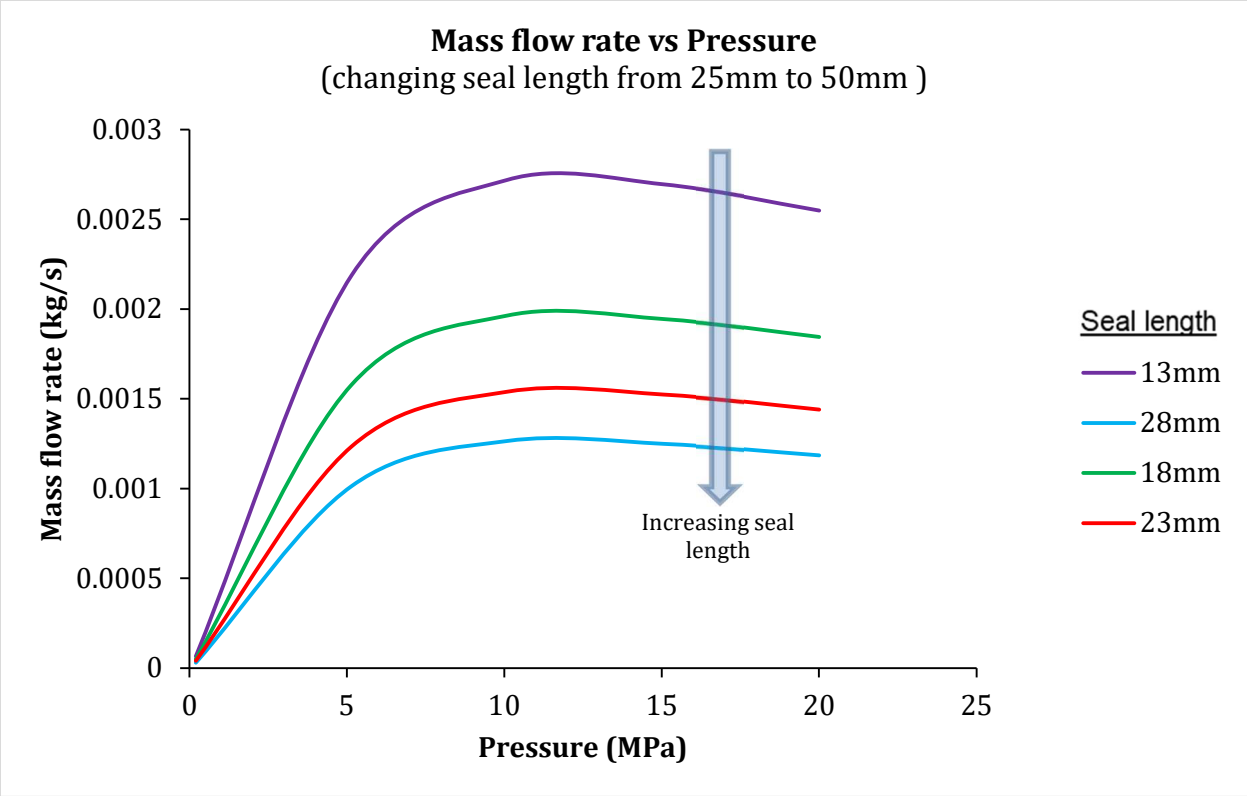

Figure 24: Mass flow rate vs Pressure plot with varying seal length

The mass flow rate vs pressure plot when the seal length is varied from 13mm to 28mm at 0.2 MPa to 20 MPa is illustrated in Figure 24 above. Applying Poiseuille's Law stating that the flow rate is inversely proportional to the length and viscosity of a body. This means that if the length of the body is doubled, the operator gets half the flow rate at the exit at constant pressure and temperature. Similar analogy is happening in this case for the seal shown in Figure 24. If a longer seal of 28mm is used, the flow resistance naturally increases in direct proportion to its length due to friction forces acting on the seal and rotating shaft resulting in a decrease in its mass flow rate. A longer seal is more desirable for sealing conditions as it would generate a lower mass flow rate, but one must consider the diameter of the shaft to be of a proportional size also as the proposed seal wraps around it in a sleeve like structure. This is the reason why a seal length of 26.50mm was chosen for this case to accommodate for the 50mm shaft diameter. When running

the MATLAB code, if you input seal lengths greater than around this length for a 50mm shaft diameter, it generates error messages as it would not be realistic in real life applications.

Table 25: Mass flow rate for varying seal length at 20MPa

Seal length	Initial pressure	Mass flow rate
13mm	20MPa	0.00255 kg/s
18mm	20MPa	0.001845 kg/s
23mm	20MPa	0.00144 kg/s
28mm	20MPa	0.001185 kg/s

Table 26: Mass flow rate for varying seal length at 10MPa

Seal length	Initial pressure	Mass flow rate
13mm	10MPa	0.002720 kg/s
18mm	10MPa	0.001965 kg/s
23mm	10MPa	0.001540 kg/s
28mm	10MPa	0.001265 kg/s

Table 27: Mass flow rate for varying seal length at 5MPa

Seal length	Initial pressure	Mass flow rate
13mm	5MPa	0.002190 kg/s
18mm	5MPa	0.001580 kg/s
23mm	5MPa	0.001235 kg/s
28mm	5MPa	0.001265 kg/s

CHAPTER 5

CONCLUSION

5.1 Conclusions

A novel EHD seal for sCO_2 application was proposed that is capable of sustaining low leakage rate, low wear, and minimal cost when subjected to high pressure and temperature operating conditions. A case study for a 2" test seal was presented. The main outcomes of this work can be summarized as follows:

- A proof-of-concept study for a novel EHD seal was presented and verified by using the Reynolds equation, Lame's formula, Dowson-Higginson formula, and Barus Equation.
- The set of nonlinear equations was solved using the ode45 function in MATLAB to determine the pressure distribution, clearance distribution, and mass flow rate.
- The pressure decreased almost linearly at low operating pressures ($P_0 < 7MPa$) from the inlet to the outlet. However, the decay in the pressure became sharper closer to the outlet at higher pressure values ($P_0 > 7MPa$).
- The clearance height decreased from the inlet to the outlet as the operating pressures increased.
- The clearance height proved that there would be a throat happening past the midpoint location of the seal.
- Results showed that the mass flow rate (or leakage rate) decreased at higher pressures with a leakage rate of 0.001615kg/s at 20MPa.
- A parametric study was conducted to observe the effects of the seal thickness, shaft diameter, and seal length on the seal performance at different operating pressures (20MPa, 10MPa and 5MPa).

- The mass flow rate decreased at higher pressures as the seal thickness decreased as shown in Figure 26. At 20MPa, the mass flow rate obtained for a seal thickness of 0.5mm and 2.0mm was 0.00161kg/s and 0.004055kg/s. At 10MPa, the mass flow rate was 0.00161kg/s and 0.00264kg/s for 0.5mm and 2.0mm respectively. At 5MPa, the mass flow rate was 0.00118kg/s and 0.00151kg/s for 0.5mm and 2.0mm. respectively.
- The mass flow rate decreased at higher pressures for a seal with a larger diameter compared to a smaller one. This is because the larger seal would deform more at higher pressures compared to a more compact smaller one. At 20MPa, the mass flow rate was 0.00187kg/s and 0.00125kg/s for a shaft diameter of 25mm and 50mm, respectively. At 10MPa, it was 0.001275kg/s and 0.001335kg/s respectively, and at 5MPa it was 0.000745kg/s and 0.001075kg/s for 25mm and 50mm shaft diameter, respectively.
- The mass flow rate decreased as the seal length increased. A longer seal would naturally have more resistance (friction) to the flow than a smaller one. At 20MPa, the mass flow rate was 0.00255kg/s and 0.001185kg/s for a seal with length 13mm and 28mm respectively. At 10MPa, the mass flow rate was 0.002720kg/s and 0.001265kg/s for the 13mm and 28mm seal lengths. At 5MPa, it was 0.002190kg/s and 0.001265kg/s, respectively.
- The proposed seal could be modified even further to reduce the leakages rates and make it a viable option in sCO_2 applications.

REFERENCES

Ahn, Yoonhan, and Jeong Ik Lee. 2014. "Study of Various Brayton Cycle Designs for Small Modular Sodium-Cooled Fast Reactor." *Nuclear Engineering and Design* 276: 128–41.

Aksit, Mahmut, Yahya Dogu, J Tichy, and Mustafa Gursoy. 2004. "Hydrodynamic Lift of Brush Seals in Oil Sealing Applications." In *40th AIAA/ASME/SAE/ASEE Joint Propulsion Conference and Exhibit*, 3721.

Atkinson, Edward, and Brent Bristol. 1992. "Effects of Material Choices on Brush Seal Performance." *Lubrication Engineering;(United States)* 48 (9).

Attia Hili, Molka, Slim Bouaziz, Mohamed Maatar, Tahar Fakhfakh, and Mohamed Haddar. 2010. "Hydrodynamic and Elastohydrodynamic Studies of a Cylindrical Journal Bearing." *Journal of Hydrodynamics* 22 (2): 155–63.

Bennett, Jeffrey A, Wisher Paudel, Andres F Clarens, Brian Weaver, and Cori Watson. 2018. "Computational Analysis of Seals for SCO2 Turbomachinery and Experimental Planning." In *Proceedings of the The 6th International Supercritical CO2 Power Cycles Symposium*.

Bidkar, Rahul A, Edip Sevincer, Jifeng Wang, Azam M Thatte, Andrew Mann, Maxwell Peter, Grant Musgrove, Timothy Allison, and Jeffrey Moore. 2017. "Low-Leakage Shaft-End Seals for Utility-Scale Supercritical CO2 Turboexpanders." *Journal of Engineering for Gas Turbines and Power* 139 (2).

Cesmeci, Sevki, Rubayet Hassan, Mohammad Fuad Hassan, Ikenna Ejiogu, Matthew DeMond, Hanping Xu, and Jing Tang. 2021. "An Innovative Elasto-Hydrodynamic Seal Concept for Supercritical CO2 Power Cycles." In *ASME Power Conference*, 85109:V001T04A002. American Society of Mechanical Engineers.

Childs, Dara W, and Christopher Ramsey. 1991. "Seal-Rotordynamic-Coefficient Test Results for a Model SSME ATD-HPFTP Turbine Interstage Seal with and without a Swirl Brake."

Chupp, Raymond E, Robert C Hendricks, Scott B Lattime, Bruce M Steinetz, and Mahmut F Aksit. 2007. "Turbomachinery Clearance Control."

Cieślewicz, Stanisław Michał. 2004. *CFD-Simulations for Advanced Turbomachinery Sealing Technologies Brush Seals*. na.

Dowson, D. 1962. "A Generalized Reynolds Equation for Fluid-Film Lubrication." *International Journal of Mechanical Sciences* 4 (2): 159–70.

Feher, Ernest G. 1968. "The Supercritical Thermodynamic Power Cycle." *Energy Conversion* 8 (2): 85–90.

Fortier, Alicia E, and Richard F Salant. 2005. "Numerical Analysis of a Journal Bearing with a

Heterogeneous Slip/No-Slip Surface."

Hunter, W B, and O C Zienkiewicz. 1960. "Effect of Temperature Variations across the Lubricant Films in the Theory of Hydrodynamic Lubrication." *Journal of Mechanical Engineering Science* 2 (1): 52–58.

Kudriavtsev, V V, and M J Braun. 1996. "Model Developments for the Brush Seal Numerical Simulation." *Journal of Propulsion and Power* 12 (1): 193–201.

Lattime, Scott Byran. 2000. *A Hybrid Floating Brush Seal (HFBS) for Improved Sealing and Wear Performance in Turbomachinery Applications*. The University of Akron.

Mertz, Alexander M. 2019. "Numerical Analysis of Lubricated Contacts." *ProQuest Dissertations and Theses*. Ann Arbor: University of Colorado at Denver. https://www.proquest.com/dissertations-theses/numerical-analysis-lubricated-contacts/docview/2288850196/se-2.

MUNSON, JOHN. 1993. "Testing of a High Performance Compressor Discharge Seal." In *29th Joint Propulsion Conference and Exhibit*, 1997.

Muszynska, Agnes. 2001. "The Fluid Force Model in Rotating Machine Clearances Identified by Modal Testing and Model Applications: An Adequate Interpretation of the Fluid-Induced Instabilities." In *Iscorma-2, International Symposium on Stability Control of Rotating Machinery, South Lake Tahoe, California*.

Myant, Connor, Mark Fowell, Hugh A Spikes, and Jason R Stokes. 2010. "An Investigation of Lubricant Film Thickness in Sliding Compliant Contacts." *Tribology Transactions* 53 (5): 684–94.

Peiran, Yang, and Wen Shizhu. 1990. "A Generalized Reynolds Equation for Non-Newtonian Thermal Elastohydrodynamic Lubrication."

Persichilli, Michael, Alex Kacludis, Edward Zdankiewicz, and Timothy Held. 2012. "Supercritical CO2 Power Cycle Developments and Commercialization: Why SCO2 Can Displace Steam Ste." *Power-Gen India & Central Asia* 2012: 19–21.

Rom, Michael, and Siegfried Müller. 2019. "A New Model for Textured Surface Lubrication Based on a Modified Reynolds Equation Including Inertia Effects." *Tribology International* 133: 55–66.

Tibos, S M, J A Teixeira, and C Georgakis. 2017. "Investigation of Effective Groove Types for a Film Riding Seal." *Journal of Engineering for Gas Turbines and Power* 139 (7).

White, Martin T., Giuseppe Bianchi, Lei Chai, Savvas A. Tassou, and Abdulnaser I. Sayma. 2021. "Review of Supercritical CO2 Technologies and Systems for Power Generation." *Applied Thermal Engineering* 185 (February): 116447. https://doi.org/10.1016/j.applthermaleng.2020.116447.

Zheng, Xiaoqing, and Gerald Berard. 2001. “Development of Non-Contacting, Film-Riding Face Seals for Large-Diameter Gas Engines.” In *37th Joint Propulsion Conference and Exhibit*, 3624.

———. 2008. “Development of Non-Contacting, Low-Leakage, Large-Diameter Air Seal.” In *44th AIAA/ASME/SAE/ASEE Joint Propulsion Conference & Exhibit*, 4507.

APPENDIX

MATLAB CODE

```
function dPdx = CalculateP ( x, Px )
%% Function for performance evaluation of high pressure sleeve seal

global P_0 Q mu_0 alpha rho_0 Elasticity d_shaft t_seal L_seal h_0 D D_0 xpartition j

% calculating Ks, h, rho, mu

k1  = D * D_0^2 / ( (D_0^2 - D^2) * Elasticity * h_0 ); %Eq(32)

k2  = k1;

mu  = mu_0 .* exp( alpha .* Px ); %Eq(34)
%mu  = mu_0;

h   = h_0 * ( 1 + (k1 * Px - k2 * P_0(j)).*(1-x/L_seal)); %Eq(31)

rho = rho_0 * ( 1 + 0.6 * Px ./ (1 + 1.7*Px) ); %Eq(33)

% calculating the dp/dx

dPdx = -12 * Q .* mu ./ (pi .* rho * D .* h.^3); %Eq(29)

```

```
clc; close all; clear global; close all; clear all; hold off;
format long
global P_0 Q mu_0 alpha rho_0 Elasticity d_shaft t_seal L_seal h_0 D D_0 xpartition p_out N j
%global j
%% Input Data
% Physical parameters

Q          = 1e-3;               % kg/s leakage flow rate
mu_0       = 0.2177;             % kg/m.s = Pa.s, dynamic viscosity
alpha      = 0.0134e-6 ;         % 1/Pa, pressure-viscosity coefficient
rho_0      = 876;                % kg/m3, density of the fluid
Elasticity = 214e9 ;             % Pa, Young's modulus of the seal
d_shaft    = 50.08e-3;           % m, diameter of the shaft
t_seal     = 0.5e-3;             % m, thickness of the seal
L_seal     = 26.50e-3;           % m, length of the seal
h_0        = 50e-6;              % m, initial seal clearance
D          = d_shaft + 2 * h_0;  % m, outer diameter of the clearance
D_0        = D + 2 * t_seal;     % m, outer diameter of the seal
p_out      = 101325;             % Pa, outlet pressure
N          = 10000;              % number of iterations
```

```
%% meshing the length and initializing P
x_0 = 0;
x_L = L_seal;
xpartition = 1000;


xspan = linspace( x_0, x_L, xpartition );
%P_0 = linspace(101325,10e6,10);
%Q_0 = linspace(1e-3,200e-3,10);
%P_0 = [101325:1013250:20e6];
%P_0 = 0.2e6;
P_0 = linspace( 0.2e6, 20e6, 10);
p = [];
m = [];
h = [];

for j=1:length(P_0)

P_initial = P_0(j);
```

```
%% Integrate the Nonlinear Ordinary Differential Equation
for i=1:N
options = odeset('RelTol', 1e-2, 'AbsTol', 1e-5);

[x1, p1] = ode45( @CalculateP, [x_0 x_L], P_initial, options );

if (p1(end)-p_out)>0 && abs(p1(end)-p_out)>1e-3
   Q = Q + 0.0025e-3;
    else
        if (p1(end)-p_out)<0 && abs(p1(end)-p_out)>1e-3
            Q = Q - 0.0025e-3;
        else
            break
end
end
end

p = [p p1];
m = [m Q];
```

```
figure (3)
plot(P_initial, Q,'r-o');
xlabel( 'Pressure (Pa)' );
ylabel( 'Mass flow rate (kg/s)' );
title( 'Mass flow rate vs Pressure' );
hold on;
grid on;

figure (1)
plot(x1, p1);
xlabel( 'Distance (m)' );
ylabel( 'Pressure (Pa)' );
title( 'Pressure distribution' );
hold on;
grid on;
```

```
figure (2);
k11  = D * D_0^2 / ( (D_0^2 - D^2) * Elasticity * h_0 );
k22  = k11;
h1   = h_0 * ( 1 + (k11 * p1 - k22 * P_initial).*(1-x1/L_seal));
plot(x1, h1);
xlabel( 'Distance (m)' );
%ylabel( 'Clearance (\mu m)' );
ylabel( 'Clearance (m)' );
title( 'Clearance distribution' );
hold on;
grid on;
```